Reprinted from:

SHOCK WAVES AND HIGH - STRAIN - RATE PHENOMENA IN METALS (1981)
Edited by Marc A. Meyers and Lawrence E. Murr
Book available from: Plenum Publishing Corporation
233 Spring Street, New York, N.Y. 10013

Chapter 30

DEFECT GENERATION IN SHOCK-WAVE DEFORMATION

Marc A. Meyers
Lawrence E. Murr

Department of Metallurgical and Materials Engineering
New Mexico Institute of Mining and Technology
Socorro, New Mexico 87801 USA

A theoretical framework elucidating the generation of shock-induced defects is presented. Three different mechanisms responsible for the generation of point, line, and planar defects (twins and stacking faults), respectively, are described. Dislocations are homogeneously nucleated at or slightly behind the shock front by the powerful deviatoric stresses generated by the shock pulse; they are accelerated by the residual deviatoric stresses either towards or away from the front. Dislocation dynamical considerations limit their velocity to the velocity of shear waves in the medium. Their self-energy and stiffness are very high at the high velocities; hence, their ability to generate point defects upon intersecting each other is greatly enhanced, because the drag stress produced by the jogs is essentially independent of the velocity.

Twinning is not thought to occur by a pole mechanism, but by the cooperative glide of partial or special dislocations along parallel planes. Nucleation may take place at stress-concentration regions either by emission of a dislocation from interfacial or surface ledges, or homogeneously in the lattice.

Displacive, diffusionless transformations can be induced either by the hydrostatic or the deviatoric components of the stress state imposed by the shock wave. In ferrous alloys, the γ(FCC) $\rightarrow$ α(BCC,BCT) transformation is shown to be both induced by intersecting arrays of dislocations and planar defects (shear strain) and by hydrostatic tensile stresses.

The effects of material parameters (alloy composition, grain size, etc.) and of shock-wave parameters (peak pressure, pulse duration, etc.) on the occurrence of point, line and planar defects are discussed in terms of the mechanisms proposed, and illustrated by observed experimental results.

I. INTRODUCTION AND SCOPE

The metallurgical effects associated with dynamic loading were first described in reasonable detail by Rinehart and Pearson (1). The first systematic investigation of the substructural changes in terms of fundamental deformation modes induced by the passage of shock waves is described in the classic paper by Cyril Smith (2); this work was conducted in cooperation with the Los Alamos Scientific Laboratory. During the past three decades, the activity in this specialized area of metallurgy has steadily continued, and a few hundred papers have resulted. Table I presents the main reviews summarizing this work. This exploratory phase of shock loading consists of a number of studies devoted to the determination of residual or *post explosionem* substructures and mechanical properties of a wide range of metals and alloys. At the same time there developed a realization that the shock-wave parameters can play an important role in the determination of these substructures and associated mechanical properties. Disagreement between different investigators seems to be, in the first stage, more the rule than the exception, and the reason for this seems to be in: (a) the lack of attention given to important shock-wave and material parameters and (b) improperly conducted experiments (10). As a result of this state of disarray, a fundamental understanding has been slow to take shape. Hence, this paper will not scan the voluminous body of work in a comprehensive and exhaustive manner.

TABLE I. Review Articles on the Metallurgical Effects of Shock Waves.

Author	*Year*	*Reference*
G.E. Dieter	*1962-63*	*3,4*
E.G. Zukas	*1966*	*5*
H.E. Otto and R. Mikesell	*1967*	*6*
R.N. Orava	*1973*	*7*
W.C. Leslie	*1973*	*8*
L. Davison and R.A. Graham	*1979*	*9*

Rather, an attempt will be made to present a modellistic framework explaining the various substructural features produced by the passage of shock waves in terms of micromechanical deformation modes. This is a necessary step towards a quantitative, theoretical understanding of the phenomena involved. Some of the concepts have been enunciated before, some are being proposed for the first time.

II. STATE OF STRESS INDUCED BY SHOCK WAVES

In order to understand the effects of shock waves on metals, it is essential to correctly identify and analyze the state of stress involved. By definition, the state of stress generated by a planar, normal shock wave (particle velocity is perpendicular to shock front) is a *uniaxial strain state* (11). This state of stress should be decomposed into a deviatoric and a hydrostatic component. The uniaxial strain state can be represented as:

$$\begin{bmatrix} d\varepsilon_1 & 0 & 0 \\ 0 & 0 & 0 \\ 0 & 0 & 0 \end{bmatrix} \qquad [1]$$

This strain can be decomposed into its hydrostatic and its deviatoric components as follows:

$$\begin{bmatrix} d\varepsilon_1/3 & 0 & 0 \\ 0 & d\varepsilon_1/3 & 0 \\ 0 & 0 & d\varepsilon_1/3 \end{bmatrix} + \begin{bmatrix} 2d\varepsilon_1/3 & 0 & 0 \\ 0 & -d\varepsilon_1/3 & 0 \\ 0 & 0 & -d\varepsilon_1/3 \end{bmatrix} \qquad [2]$$

The corresponding stresses are [using Eqs. 2.75 and 2.76 of ref. (12)], for an isotropic material:

$$\begin{bmatrix} \frac{E}{3(1-2\nu)}d\varepsilon_1 & 0 & 0 \\ 0 & \frac{E}{3(1-2\nu)}d\varepsilon_1 & 0 \\ 0 & 0 & \frac{E}{3(1-2\nu)}d\varepsilon_1 \end{bmatrix} + \begin{bmatrix} \frac{2Ed\varepsilon_1}{3(1+\nu)} & 0 & 0 \\ 0 & \frac{-Ed\varepsilon_1}{3(1+\nu)} & 0 \\ 0 & 0 & \frac{-Ed\varepsilon_1}{3(1+\nu)} \end{bmatrix} \qquad [3]$$

It should be emphasized that Eqs. [1-3] assume elastic behavior of the material; it is assumed here that the material is responding elastically to the passage of the wave. This matter will be discussed further in Section II, C. The pressure is the hydrostatic component:

$$dP = \frac{E}{3(1-2\nu)} d\varepsilon_1 \quad [4]$$

dP is an elastic hydrostatic stress; the original dimensions of the specimen would be recovered, once dP were released. If one wants to know the total pressure, P, after an extensive deformation ε_1, one has:

$$\int_{P_0}^{P} dP = \int_{0}^{\varepsilon_1} \frac{E}{3(1-2\nu)} d\varepsilon_1 \quad [5]$$

But $d\varepsilon_1 = dL/L_0 = dV/V_0$ and $\varepsilon_1 = \ell n(V/V_0)$. This is due to the fact that the state of strain is uniaxial. The typical Hugoniot plots obtained for different materials show that the ration $E/3(1-2\nu)$ increases with increasing pressure: this can be seen from the expression:

$$\frac{dP}{(\frac{dV}{V_0})} = \frac{E}{3(1-2\nu)} \quad [6]$$

Figure 1 shows a typical P versus V/V_0 curve; the slope increases as P increases. The second term of importance in Equation [3] is the deviatoric stress. The maximum shear stresses can be found from the deviatoric stresses and occur at 45° to the shock front.

$$d\tau_{max} = \frac{1}{2}\left(\frac{2\ E\ d\varepsilon_1}{3(1+\nu)} + \frac{E\ d\ \varepsilon_1}{3(1+\nu)}\right) = \frac{1}{2}\ \frac{E\ d\ \varepsilon_1}{(1+\nu)} \quad [7]$$

Substituting Equation [4] into Eq [7]:

$$d\tau_{max} = \frac{3(1-2\nu)\ dP}{1+\nu} \quad [8]$$

Integration yields:

$$\tau_{max} = \frac{3(1-2\nu)\ P}{1+\nu} \quad [9]$$

Equation [9] can also be expressed as:

$$\tau_{max} = \frac{2G\ P}{K} \quad [10]$$

where G and K are the rigidity and bulk moduli, respectively, K is the slope of the P versus V/V_0 curve in Figure 1 [$K = E/3(1-2\nu)$]. From Eq. [6]:

$$K = \frac{dP}{dV/V_0}$$

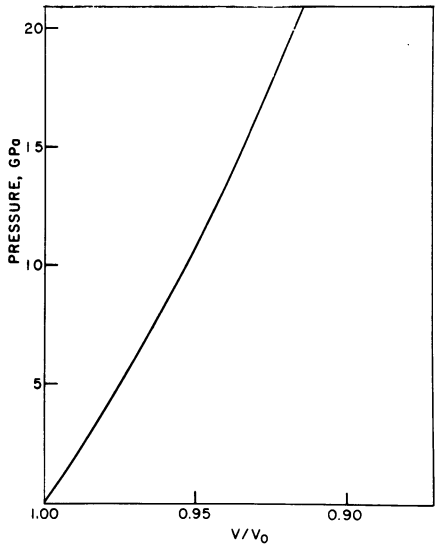

FIGURE 1. Dynamic compressibility curve for nickel (13).

From G and K, it is possible to know the maximum shear stress. This is calculated here for nickel from data presented by Bridgman (14) and Jesser and Kuhlmann-Wilsdorf (15) (Figure 2). Figure 3 presents the relationship between maximum deviatoric and hydrostatic stresses. This calculation, which is somewhat more

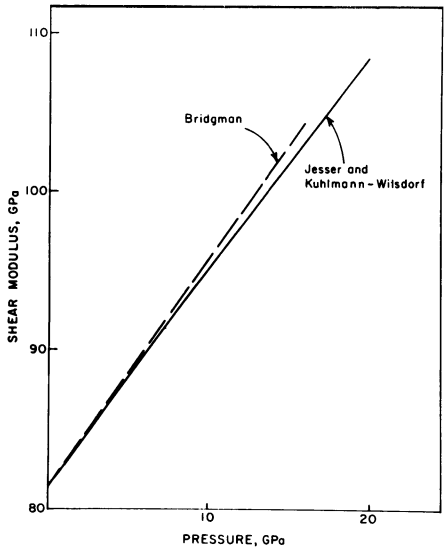

FIGURE 2. Effect of pressure on the shear modulus of nickel.

elaborate than the one presented previously by Meyers (31), shows that τ_{max} varies between 85% and 70% of P. The material cannot

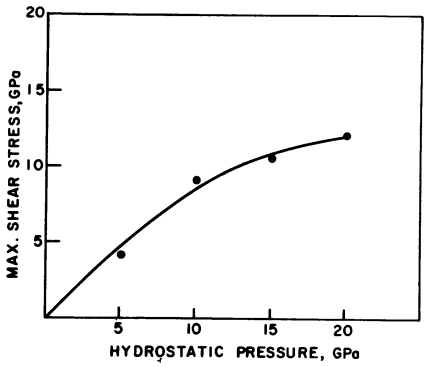

FIGURE 3. Relationship between hydrostatic and deviatoric stresses for nickel.

withstand these high shear stresses at the higher pressures; hence, they will not reach these high values, and plastic deformation will ensue. This will be discussed in detail in Section III.D.

The importance of separating deviatoric from hydrostatic stresses cannot be over emphasized. Different phenomena are controlled by different stresses. Hence, one has:

dislocations: generation and motion controlled by deviatoric stresses; stacking-fault energy affected by hydrostatic stresses.

dispersed particles: they are a source of dislocations due to the different compressibilities; hence, this is an effect of hydrostatic stresses.

individual grains: in materials that do not exhibit cubic symmetry, individual grains have anisotropic compressibilities and hydrostatic stresses will establish compatibility stresses at their interfaces.

displacive diffusionless phase transformation: a number of phase transformations are induced in materials by the hydrostatic component of stress (17). Martensitic transformation can also be induced by shear stresses or strains.

twinning: activated by shear stresses. The hydrostatic stresses might have an indirect effect.

point defects: their generation is due to shear stresses; their diffusion rate is affected by hydrostatic stresses.

recovery and melting point: affected by hydrostatic stress.

shock and residual temperatures: affected by both hydrostatic and deviatoric stresses, but for different reasons.

III DISLOCATION GENERATION

The dislocation substructures generated by shock loading depend on a number of shock-wave and material parameters. Among the shock-wave parameters, the pressure is the most important one. As the pressure is increased, so does the dislocation density. This has been shown by a number of investigators (See Chap. 38). As the dislocation density increases for high stacking-fault energy FCC metals, the cell size decreases. Murr and Kuhlmann-Wilsdorf (18) found that the dislocation density varies as the square root of pressure ($\rho \propto P^{\frac{1}{2}}$). This dependence breaks down at pressures close to 100 GPa, due to shock-induced heating.

The effect of pulse duration has been and remains to some extent, the object of controversy. Its effect for various alloys, is reviewed in ref. 19 and discussed in detail in Chapter 42. Appleton and Waddington (16) were the first to suggest its importance. The authors share the view that pulse duration does not have a significant effect on dislocation density.

The effect of pulse duration is principally to allow more time for dislocation reorganization. The cell walls become better defined as the pulse duration increases, because there is more time for dislocation reorganization. Experimental observations at very low pulse durations do not seem to be in line with the above rationalization. Mikkola and coworkers (20) have observed dislocation density increases with increasing pulse duration in the sub-microsecond range. However, in Chapter 42, Murr discusses the possiblility that these effects are due to subtle pressure variations. There are some systematic differences and similarities between shock-induced and conventionally-induced dislocations; some of these will be briefly reviewed here. In FCC metals, the stacking-fault energy determines the substructure to a large extent. In any case, however, the dislocations seem to be more uniformly distributed in shock than in conventional deformation. In high-stacking fault energy alloys, the cell walls tend to be less well-developed after shock loading than after conventional deformation, especially by creep or fatigue, which allow time for dislocations to equilibrate into more stable configurations.

Figure 4 shows the substructure of shocked (a) and cold-rolled (b) aluminum (21). It can be seen that the distribution of dislocations is much more uniform in shocked aluminum, while the cold-rolled material exhibits sub-grain boundaries. It should be noticed that the shock substructure of aluminum is not too typical of FCC metals with high stacking-fault energy. The more common feature is a cell-like structure with poorly defined cell walls, shown in Fig. 5. In addition, if the shock pulse duration is low, the substructures are more irregular because there is insufficient time for the dislocations generated by the peak pressure (in the shock front) to equilibrate (18). There is usually a preponderance of dislocation loops associated with the residual shock microstructures, and this is largely unique to shock loading of high stacking-fault free energy metals and alloys. At shock pressures above about 10 GPa, most FCC metals having stacking-fault free energies

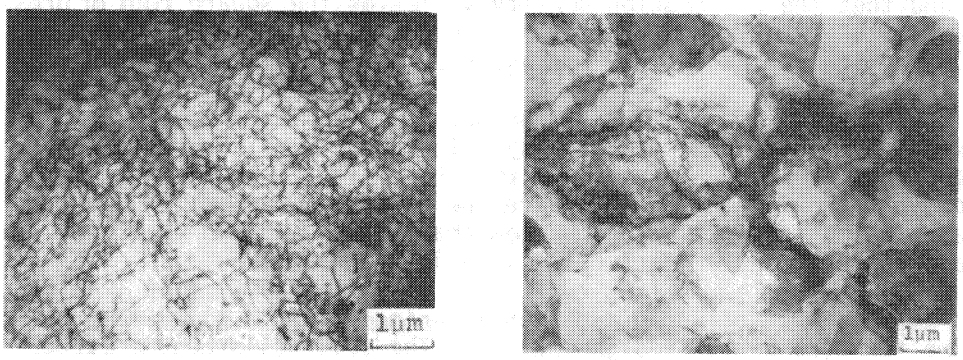

FIGURE 4. Comparison of dislocation substructures in shock-loaded and cold-rolled aluminum. (a) Aluminum shock loaded at 3 GPa peak pressure, 2 μs pulse duration. (b) Aluminum cold-roll - reduced 60%. The microstructure is dominated by sub-grain boundaries or low-angle (low-energy) dislocation interfaces.

above about 50 mJ/m^2 tend to exhibit dislocation cell structures. Between about 40 mJ/m^2 and 60 mJ/m^2 a transitional range gives rise to tangles of dislocations, poorly formed cells, and sometimes more planar arrays of dislocations (associated with the {111} slip planes).

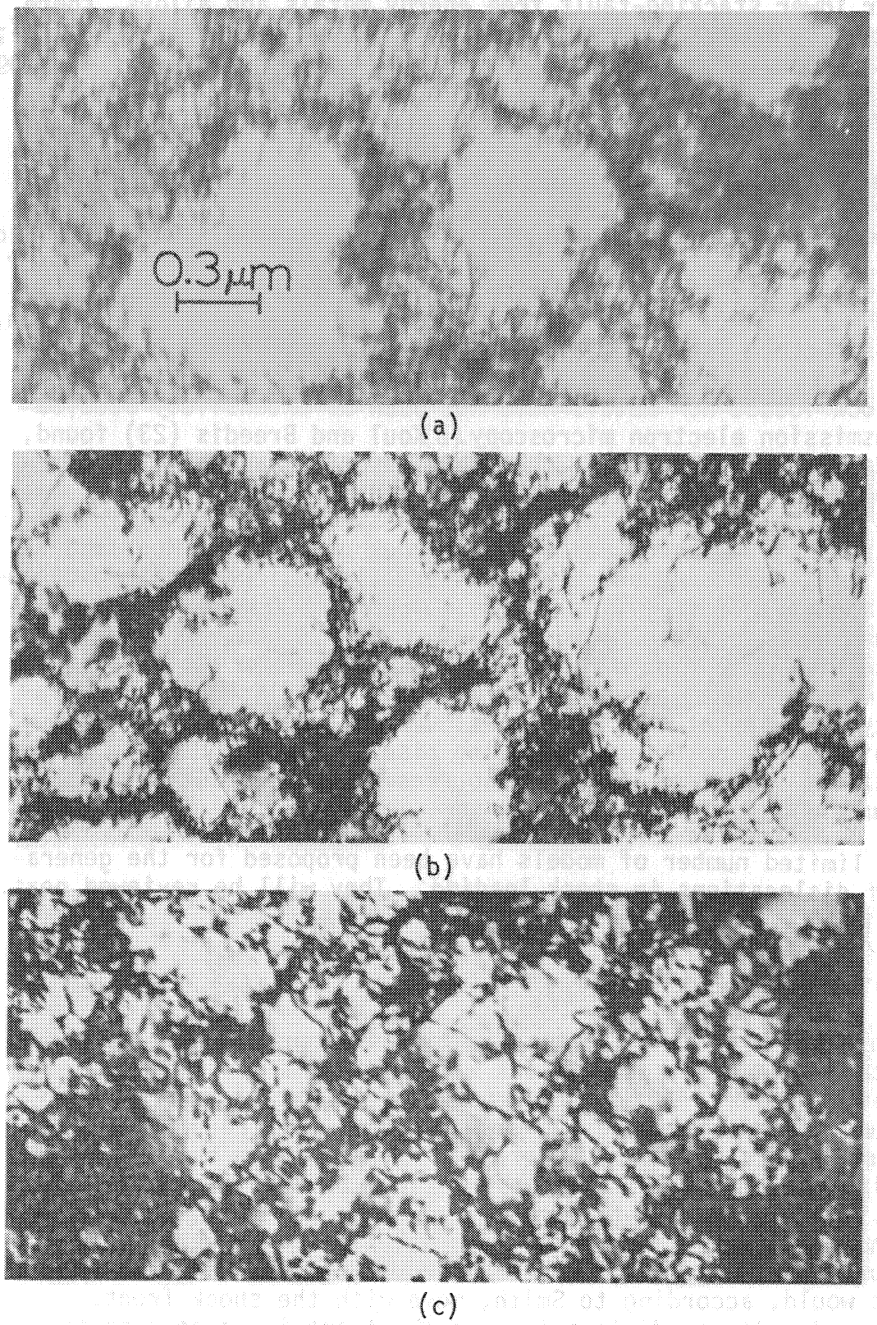

FIGURE 5. Dislocation substructures in high stacking-fault free energy FCC metals and alloys. (a) Copper shock loaded at 5GPa; 2 μs; (b) Nickel shock loaded at 10 GPa, 2 μs; (c) Fe-34% Ni shock loaded at 10 GPa, 2 μs.

For lower stacking-fault free energy metals and alloys, there is a tendency toward planar dislocation arrays below about 40 mJ/m^2; with stacking faults and twin faults becoming prominent for stacking-fault free energies below about 25 mJ/m^2. This is illustrated in Fig. 6 for 70/30 (cartridge) brass, 304 stainless steel, and an Fe-Cr-Ni alloy, each shock loaded to roughly the same pressure, at the same pulse duration.

The effect of shock loading on BCC metals is illustrated in Fig. 7 for (a) iron and (b) molybdenum. Shock loaded iron is characterized, at pressures below 13 GPa, by arrays of straight and parallel screw dislocations, in the grains properly oriented. In molybdenum, the substructure is one of homogeneously distributed dislocations.

Shock loaded HCP metals have not been as extensively studied by transmission electron microscopy. Koul and Breedis (23) found, at 7 GPa, dislocation arrays that they described as being intermediary between those of FCC metals such as Cu and Ni, and BCC metals such as iron and Fe_3Al (Fig. 7). The substructure also exhibited twins and phase transformations, at higher pressures. Murr and Galbraith (24) studied shock-loaded beryllium which exhibited dislocation substructures similar to those ones of BCC metals (Fig. 8). No twins were observed up to a pressure of 0.9 GPa. A strong dependence of dislocation density was noted for grain boundary structure. This feature is consistent with the establishment of compatibility stresses at the interfaces due to the anisotropy of compressibility, as noted above, giving rise to a preponderance of dislocations from grain-boundary sources as well as alterations in the boundary structure.

A limited number of models have been proposed for the generation of dislocations in shock loading. They will be reviewed next.

A. Smith Model (2)

Smith (2) made the first attempt to interpret the metallurgical alterations produced by shock waves in terms of fundamental deformation modes. He depicted the interface as an array of dislocations that accommodate the difference in lattice parameter between the virgin and the compressed material. In this sense the Smith interface resembles an interface between two phases in a transformation; the interface is shown in Fig. 9(b). Figure 9(a) shows the interface if no dislocations were present; the deviatoric stresses cannot be relieved. This interface of dislocations would, according to Smith, move with the shock front. Since the density of dislocations at the front is, according to Smith, 10^3 to 10^4 times higher than the residual density, sinks and sources, moving at the velocity of the shock, were postulated.

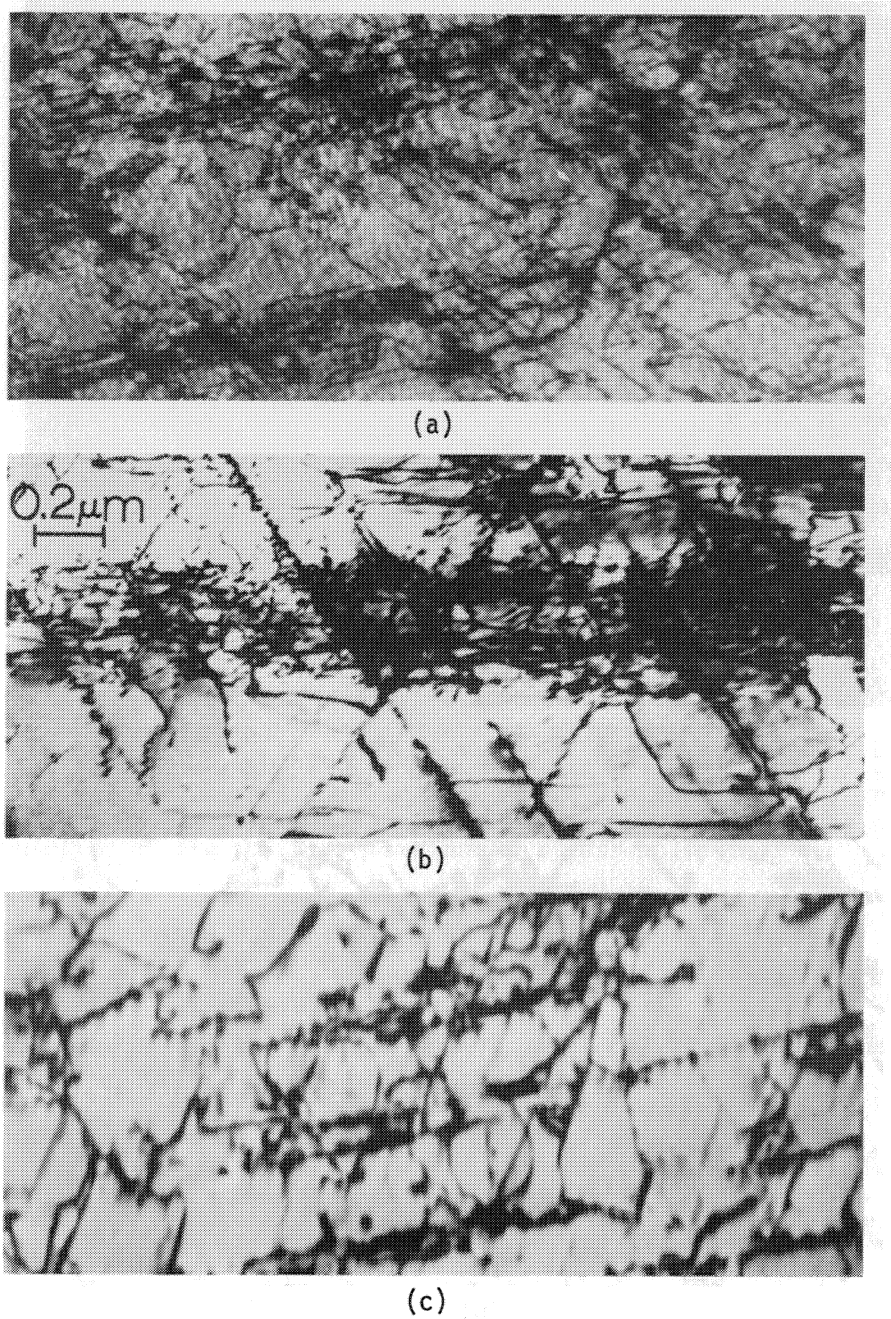

FIGURE 6. Dislocation substructures in low stacking-fault free energy FCC alloys (a) 70/30 brass shock loaded at 5 GPa, 2 μs; (b) 304 stainless steel shock loaded at 15 GPa, 2 μs; (c) Fe-15% Cr, 15% Ni alloy shock loaded at 10 GPa, 2 μs.

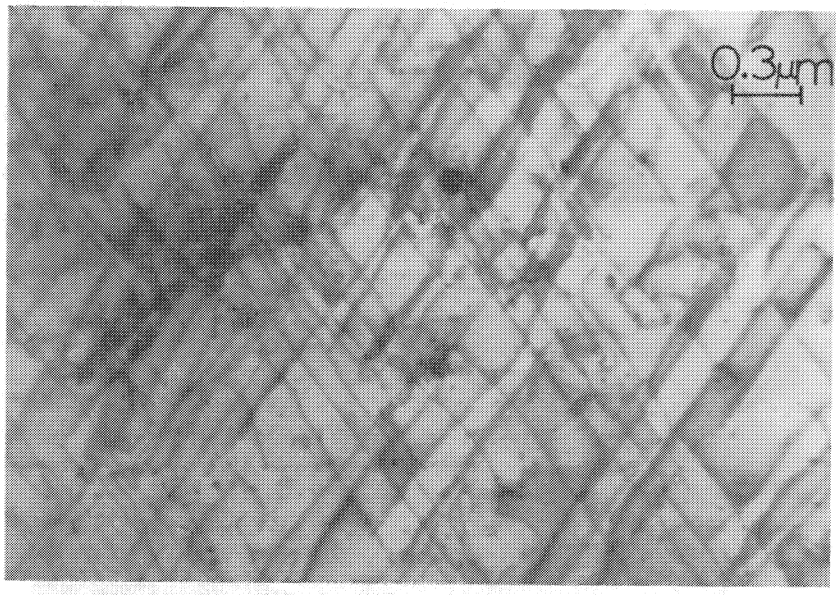

(a)

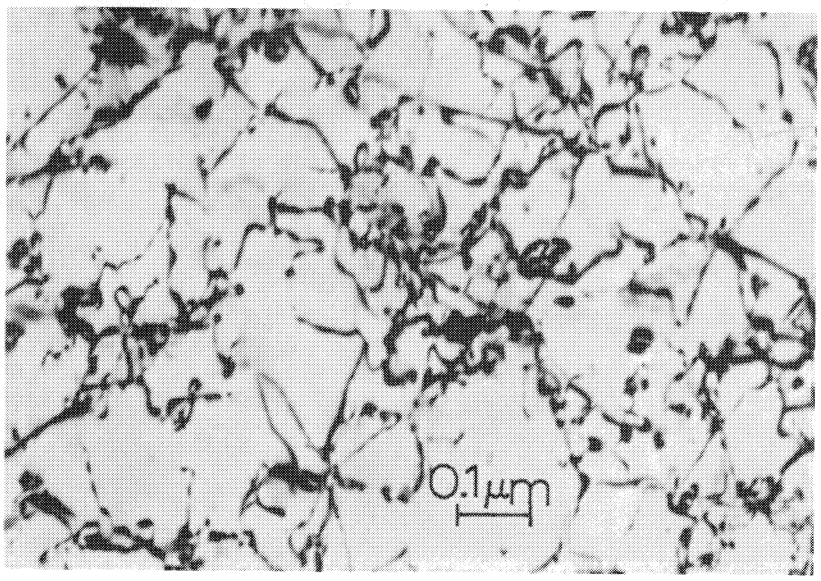

(b)

FIGURE 7. Dislocation substructures in shock-loaded BCC metals. (a) Iron shock-loaded at 7 GPa peak pressure (22) Courtesy of W.C. Leslie, (b) Molybdenum shock loaded at 15 GPa, 2 μs.

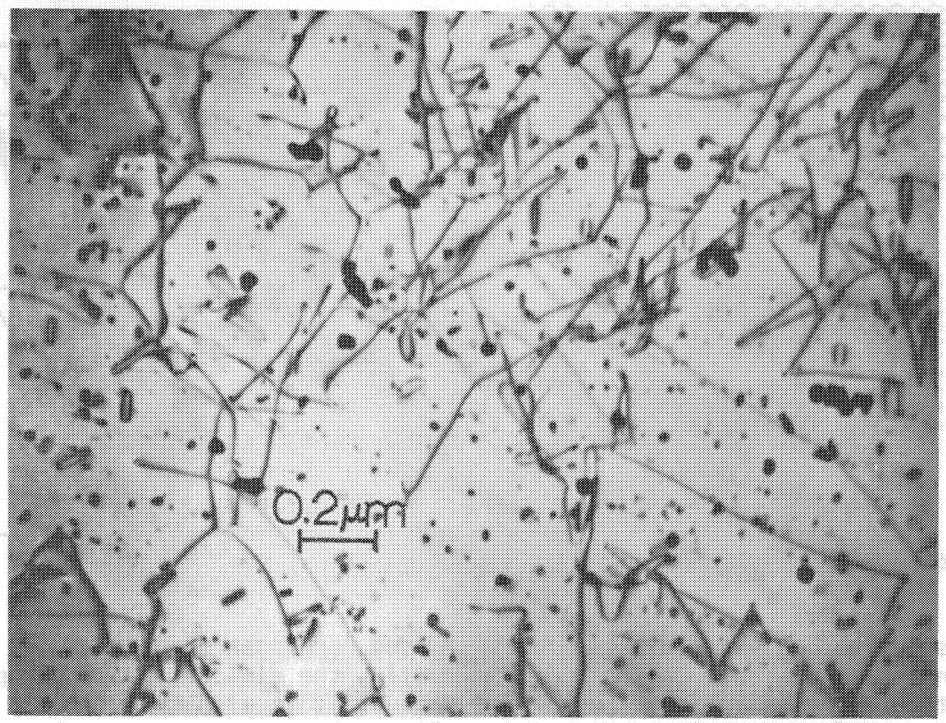

FIGURE 8. Dislocation substructure in beryllium shock loaded at a peak pressure of 0.9 GPa. Note the preponderance of large dislocation loops. The black specks are impurity artifacts accumulating on the foil surfaces during electropolishing.

B. Hornbogen's Model (25)

Hornbogen (25) modified Smith's (2) model, because it could not account for the dislocation substructures found by the former in shock-loaded iron. Figure 7(a) shows a typical microstructure, and one can see the screw dislocations lying on <111> directions. Hornbogen's explanation is shown schematically in Figure 9(c); dislocation loops are formed as the compression wave enters the crystal; the edge components move with the velocity of the shock front, so that their compression zone forms the compression zone of the wave; screw components remain and extend in length as the edge components advance.

C. Criticism of Smith's and Hornbogen's Models

Hornbogen (25) based this model on the observation of only one metal; iron. Different metals and alloys exhibit widely different

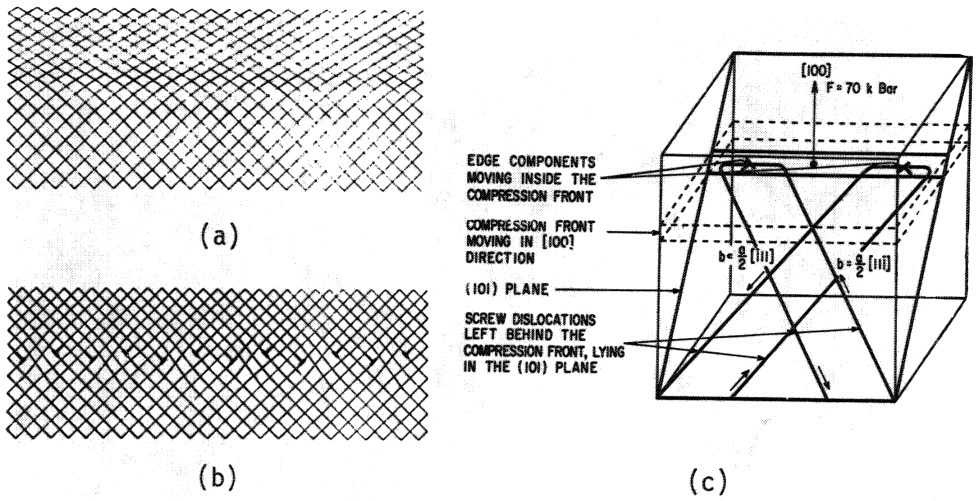

FIGURE 9. Smith (a,b) and Hornbogen's(c) models for dislocation generation on shock loading.

substructures as shown in Figs. 4-8, and Hornbogen's model would not be applicable to them. Additionally, the dislocation substructure depicted in Fig. 7(a) is not unique; it is also typical of iron deformed at low temperature. Figure 10 shows for comparison the substructure obtained by deforming iron at 77K; it is almost identical to that of shock-loaded iron. Indeed, the shock-loaded substructures tend to resemble the low-temperature substructures induced by conventional deformation. The large incidence of screw dislocations is indicative of their low mobility at low temperature; this topic is discussed in greater detail in references 26 and 27. This phenomenon is characteristic of BCC metals, and is the reason for the large temperature dependence of their flow stress at low temperatures.

Smith's model requires dislocations moving with the shock front; it will be shown, for a specific example, that this requires supersonic dislocations. Figure 11 shows the velocity of a dislocation as a function of its orientation with respect to the shock front. Calculations were conducted for nickel being shocked at 9.4 GPa. V_s, the velocity of an elastic shear wave at the above pressure, was taken as the unit. The velocity of the dislocation (independent of orientation) in a Smith or Hornbogen interface substantially exceeds V_s.

Many attempts have been made to fit the velocity-stress relationships to mathematical equations. Although the experimental results are fragmented, they allow a more general conclusion to be drawn:

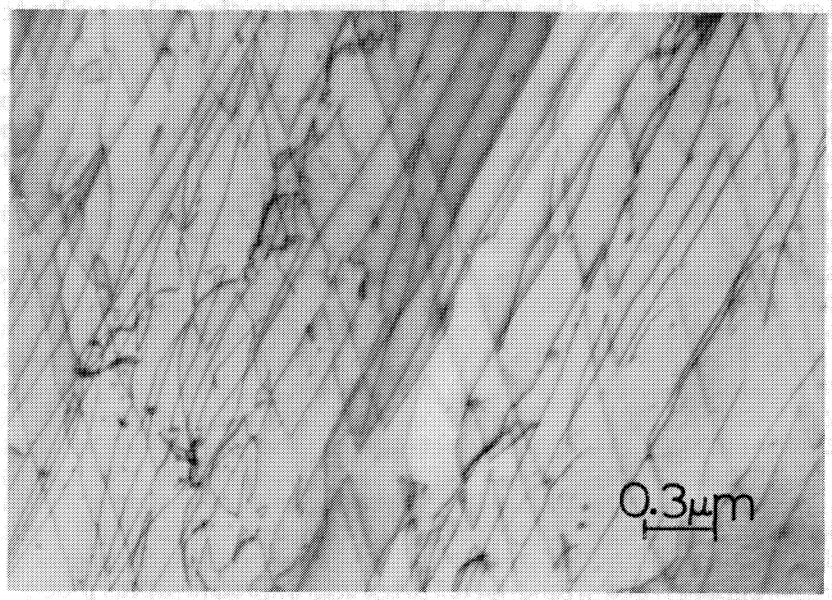

FIGURE 10. Transmission electron micrograph of iron conventionally deformed at 77K (22). (Courtesy of W.C. Leslie)

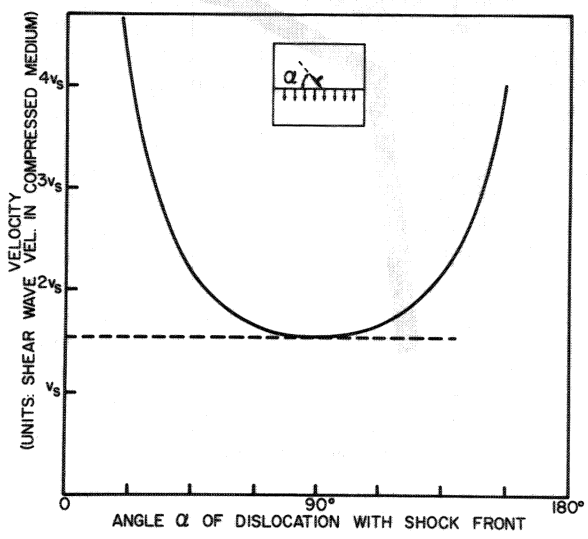

FIGURE 11. Velocity of dislocation in Smith interface as a function of orientation with shock front.

the slope decreases as the velocity increases, in a log velocity-log stress plot (the stresses being plotted on the abscissa). This is shown in ref. 28. If one wants to predict the response of nickel, experimentally determined by Rohde and Pitt (29) for low velocities, one should observe that, in the medium velocity range, the velocity and stress have been found by several investigators to be linearly related through a viscous damping coefficient. (In the log-log plot of Figure 3 of ref. 28, this corresponds to the unit slope). Figure 12 shows a hypothetical prediction of the stress dependence of dislocation velocities in nickel, in accord with the aforementioned observations. It can be seen that the stress required to move a dislocation at a velocity equal to the sound velocity is infinite. Another extremely important aspect of dislocation motion is that no supersonic dislocations have been observed, to this date. This is in line with the relativistic effects (infinite dislocation self-energy when velocity becomes equal to the shear velocity of sound) and the phonon scattering ideas. These authors share with Friedel (30) the idea: "A dislocation moving under a constant applied external stress cannot exceed the speed of sound c. For it is a signal which can be Fourier analyzed into plane waves of strain (sound waves, or phonons), and one knows that a signal cannot travel faster than the waves that carry it".

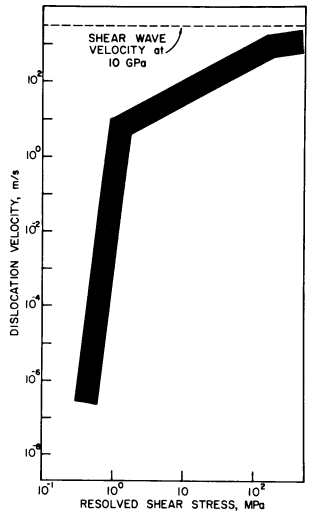

FIGURE 12. Velocity of dislocation in nickel as a function of applied stress (Extrapolated from Rohde and Pitt (29).

A few simple calculations will show that the energy released by a moving Smith-Hornbogen interface would be of such a magnitude that exceedingly high temperatures would be generated. Let us assume that nickel is being shock-loaded at 10 GPa. The ratio between compressed and uncompressed specific volumes is 0.953; the density of dislocations geometrically required along the Smith interface is determined from the misfit between the two lattices (the virgin and compressed one). Following the calculations delineated in ref. 31, one finds that one has one dislocation doublet for every 21.3 unit cells, or one dislocation for every 53A. The work involved in moving them is given by the Peach-Koehler equation:

$$W = \tau b \ell \qquad [11]$$

where τ is the applied shear stress, b, the Burgers vector (3.5×10^{-10} m) and ℓ is the distance moved by each dislocation. A pressure of 10 GPa generates a shear stress of 9.25 GPa (Fig. 3); this is the shear stress driving the interfacial dislocations. It is assumed that the dislocations are at an angle of 45° with the shock front; they consequently move 1.41 cm when the front advances 1 cm. The work, per dislocation and per cm of front advance is equal to 5.8×10^{-6} J. The work per cm^3 is obtained by multiplying W by the dislocation density along the front. In order to compute it, one has to consider the two-dimensional grid of dislocations at the front. So, the number of dislocations per cm^2 of front is equal to 3.77×10^6, or a total length of 3.77×10^6 cm. The total work to move them is equal to 21.9 J. Assuming that all this energy is dissipated as heat, one obtains (density is 8.87 g/cm^3 and heat capacity equal to 0.44 J/Kg) a temperature increase of 441K. For pressures of 15 and 20 GPa one obtains, repeating the calculations, residual temperature rises of 717 and 1045 K, respectively. However, experimental observations by McQueen, et al. (33) and Taylor (32) show that the residual temperatures in iron and copper, respectively do not differ too much from thermodynamic predictions; this is shown in Fig. 13(a) and (b). The full lines indicate the predictions from hydrodynamic theory. The measured residual temperatures tend to be equal to or higher than the calculated values (assuming that there are no internal, dissipative processes in the material). Recent experimental results by Raikes and Ahrens (98) for aluminum and stainless steel confirm this. This strongly suggests that there is no Smith interface in shock-loaded metas.

D. Meyers Model (28,31)

The limitations of Smith and Hornbogen's proposals led Meyers (28,31) to propose a model whose essential features are:

a) Dislocations are homogeneously nucleated at (or close to) the shock front by the deviatoric stresses set up by the state of

uniaxial strain; the generation of these dislocations relaxes the deviatoric stresses.

b) These dislocation move short distances at *subsonic speeds*.

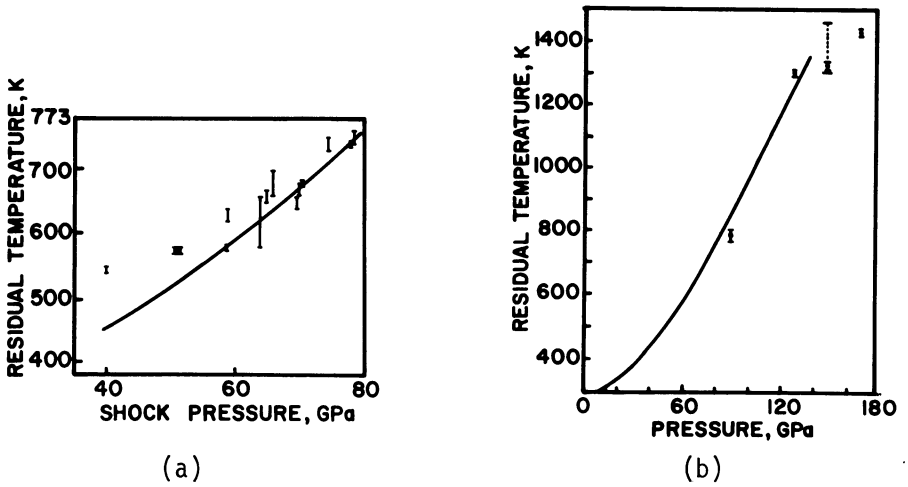

FIGURE 13. Experimentally determined and residual temperatures in shock-loaded iron (a) and copper (b) (From refs. 33 and 32 respectively).

c) New dislocation interfaces are generated as the shock wave propagates through the material.

This model presents, with respect to its predecessors, the following advantages:

a) No supersonic dislocations are needed.
b) It is possible to estimate the residual density of dislocations.

Figure 14 shows the progress of a shock wave throughout the material in a highly simplified manner. As the shock wave penetrates into the material, high deviatoric stresses effectively distort the initially cubic lattice into a monoclinic lattice. When these stresses reach a certain threshold level, homogeneous dislocation nucleation can take place. Hirth and Lothe (34) estimate the stress required for homogeneous dislocation nucleation. The nucleation mechanism at the shock front is unique, and different from homogeneous nucleation in conventional deformation. In shock loading, the dislocation interface separates two lattices with different parameters. However, it will be assumed that the stress required is the same, (as a first approximation). From Hirth and Lothe (34) one has:

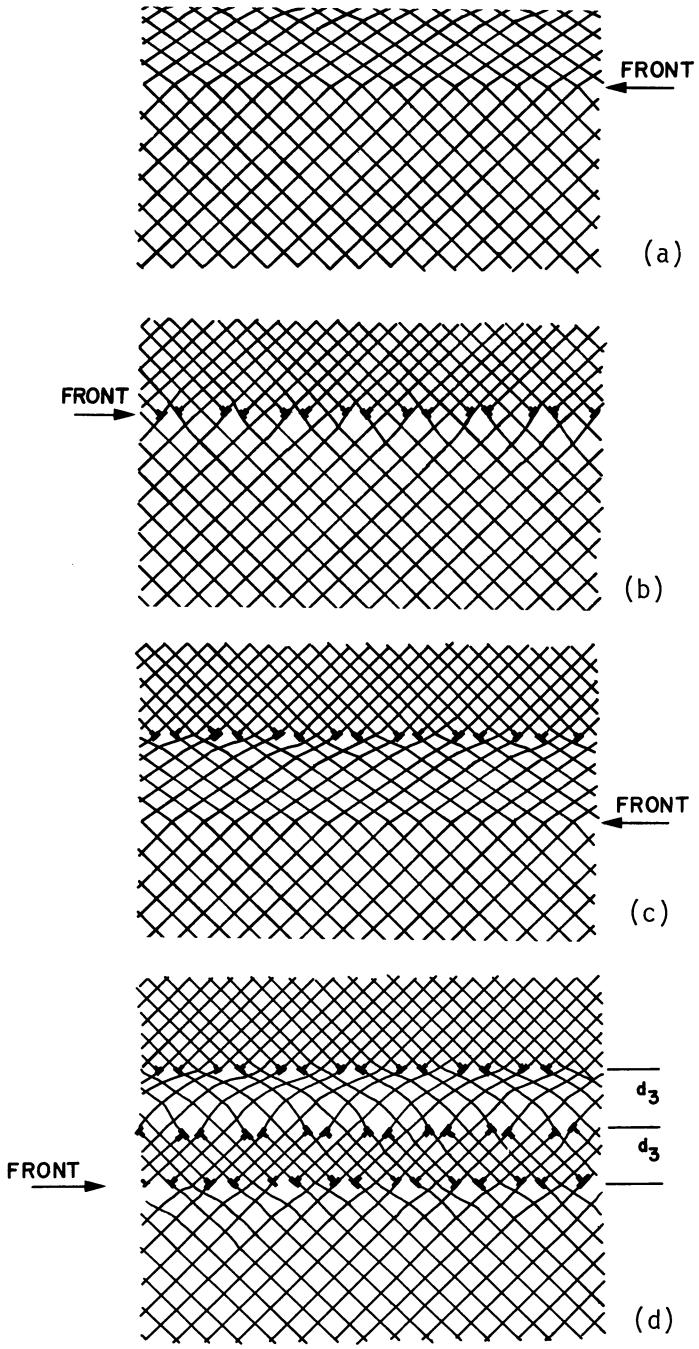

FIGURE 14. Progress of shock front according to Meyers model.

$$\frac{\tau_h}{G} = 0.054 \qquad [12]$$

τ_h is the shear stress required and G is the shear modulus, which is pressure-dependent (Figure 2). When the maximum shear stress becomes equal to τ_h (and is acting in the correct orientation), homogeneous dislocation nucleation takes place. Substituting Equation [10] into Eq. [12] one obtains:

$$P = 0.027\ K \qquad [13]$$

This value can be obtained from Figure 1 by trial and error. It corresponds to a pressure of approximately 6 GPa. Figure 14(b) shows the wave as the front coincides with the first dislocation interface. The density of dislocations at the interface depends on the difference in specific volume between the two lattices and can be calculated therefrom. In Figure 14(c) the front has moved ahead of the interface and the deviatoric stresses build up again; other layers are formed in Figure 14(d). It should be noticed that since the macroscopic strain is ideally zero after the passage of the wave, the sum of the Burgers vectors of all dislocations has to be zero. This is accomplished, in the simplified model presented here, by assuming that adjacent dislocation layers are made of dislocations with opposite Burgers vectors. Figure 15 shows two adjacent layers under the effect of shear stresses still existing in the lattice after the dislocations were nucleated; a group of dislocations move away from it. It is possible to estimate the

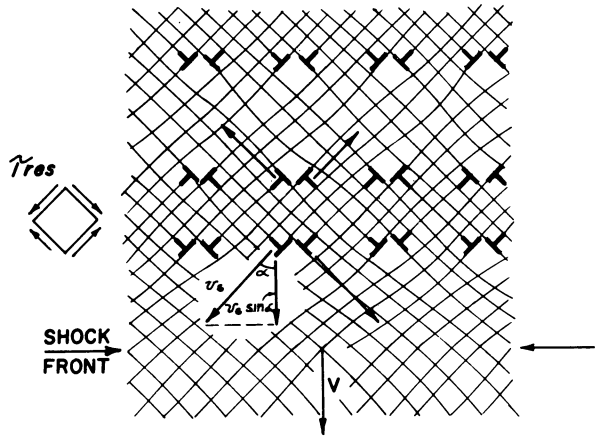

FIGURE 15. Movement of dislocations generated at the shock front (28).

velocity at which these dislocations move if one knows τ_{res}. As these dislocations move they locally accommodate and decrease τ_{res}. The total amount of internal friction and heat generation due to dislocation motion can be calculated by knowing the difference between the measured and the thermoydnamically - calculated residual temperature. A simplified calculation is presented by Hsu, et al.(35). Greater details of the model as well as comparisons of calculations with measured dislocation densities are presented elsewhere (24,25).

Recent experimental results (35,36) lead the authors to believe that the rarefaction part of the wave plays only a minor role in dislocation generation. The main reason for this is that the rarefaction part of the wave enters into a material that is already highly dislocated. It was found that (35,36) when nickel is shock-loaded repeatedly the increase in dislocation density is much less pronounced for the succeeding events. The shock wave passing through a highly dislocated material is not such an effective dislocation generator. This is consistent with Meyers' predictions (31) ... "that if a pre-strained material is shock-loaded, part of the deviatoric stresses at the shock front could be accommodated by existing dislocations; in this case the number of dislocations that would be generated at the front would be reduced. The same argument can be extended to the rarefaction portion of the wave; it can accommodate the deviatoric stresses by the movement of the existing dislocations. Additionally, the time interval in which attenuation takes place is much higher than in which the shock front rises; 200 ns versus 1 ns".

By using a different approach, Mogilevskii (34, 38) independently reached some conclusions similar to those presented here. Computer calculations using a Born-Meyer potential for the atoms allowed Mogilevskii (37) to follow the position of atoms with time. Although a perfect lattice of copper remained elastic up to pressures of 30 GPa, the introduction of point defects allowed the deviatoric stresses to be relaxed by stacking-fault (and, possibly, dislocation) generation at pressures as low as 5 GPa. Hence, Mogilevskii (37,38) was able to show how dislocations are homogeneously nucleated during the passage of a shock wave.

IV. POINT-DEFECT GENERATION

The experimental investigations conducted to date (39-46) are unanimous in indicating that shock loading produces a high density of point defects. The dynamic strain induced by shock loading is usually represented by

$$\varepsilon_s = \frac{4}{3} \ln \frac{V}{V_o} \qquad [14]$$

This corresponds to the sum of the strains imparted by the shock front and the rarefaction part of the wave. In the first systematic comparison between point defects generated by shock loading and cold rolling, Kressel and Brown (39) reported vacancy and interstitial concentrations three to four times higher after shock loading than after cold rolling. Figure 16 reproduces these results. However, direct quantitative evidence of vacancies and vacancy-type defects was obtained for the first time by Murr et al. (16). Figure 17 shows some of the vacancy loops in shock-loaded molybdenum. Field-ion microscopy showed that these loops accounted for only a small portion of the shock-induced vacancies; the majority exist as single vacancies or small clusters difficult to resolve by conventional electron microscopy.

It is relatively simple to understand why shock loading induces a large concentration of point defects. The primary source of point defects is the non-conservative motion of jogs. These jogs are generated by the intersection of screw or mixed dislocations. A few simple calculations will be conducted below in order to estimate the concentration of point defects. Figure 15 shows the direction of motion of dislocations under the effect of the residual shear stresses. As they move, τ_{res} decreases, but in the process the dislocations intersect each other, generating jogs. The non-conservative motion of these jogs produces strings of

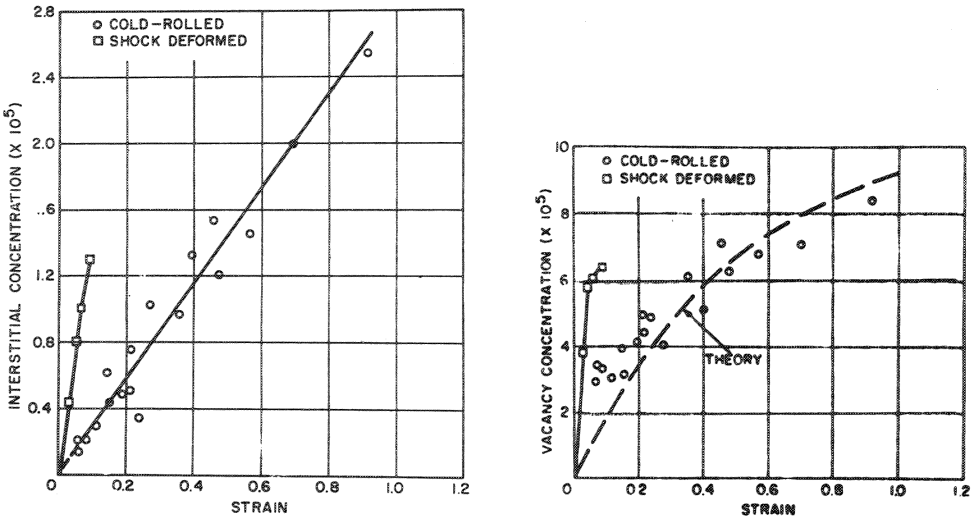

(a) (b)

FIGURE 16. Comparison between estimated interstitial (a) and vacancy (b) concentrations in nickel deformed by shock loading and conventional rolling to different strains (39).

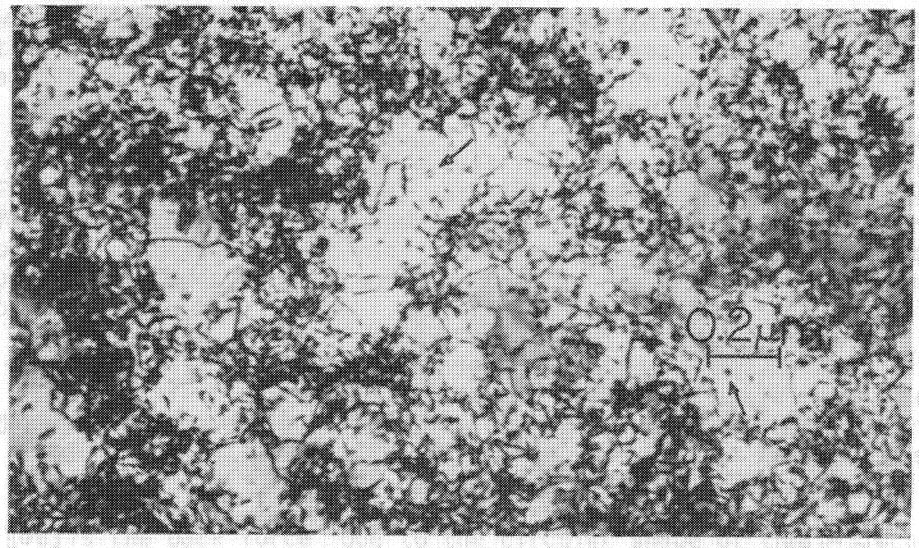

(a)

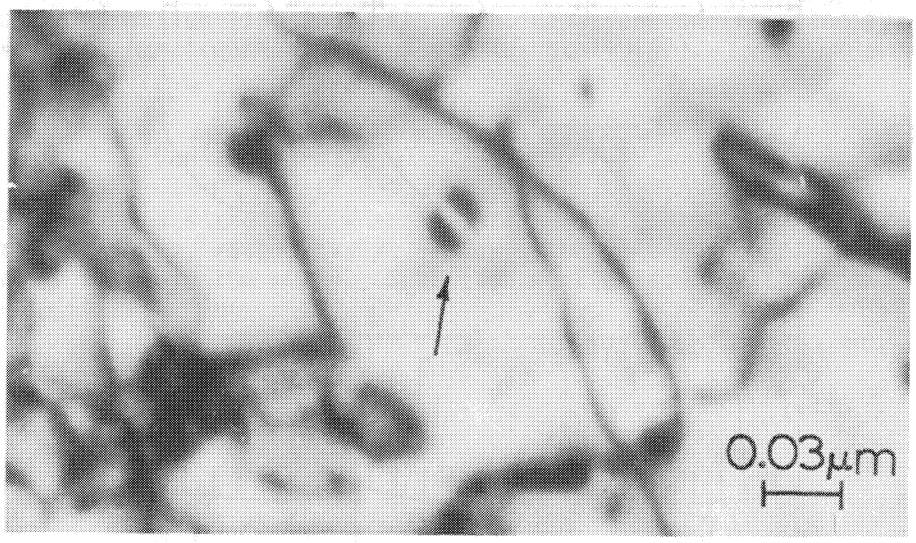

(b)

FIGURE 17. Vacancy-type dislocation loops (arrows) observed in shock-loaded metals. (a) Nickel shock-loaded at 30 GPa, 2 μs; (b) Molybdenum shock loaded at 15 GPa, 2 μs.

either vacancies or interstitials. These can also occur as dislocation loops when observed in the electron microscope as shown in Figs. 8 and 17. The subject is treated in detail by Hirth and Lothe (34); however, for the purposes of this model, a much more simplified approach will be used. Figure 18 shows dislocations containing jogs. Assuming equilibrium of forces, the force due to the applied stress τ_{AP} is balanced by the friction force F_f, the force due to the jogs, F_p, and the force due to the binding of the dislocation, F(r). Hence:

$$F_{AP} - F_f - \frac{F_p}{\ell} - F(r) = 0 \qquad [15]$$

It is assumed, sensibly, that acceleration is very high and that the equilibrium state is reached instantaneously. The frictional forces (mainly, phonon and electron drag) are dependent on velocity. One can assume a constant, viscous drag acting on the dislocation; to a first approximation:

$$F_f = Bv \qquad [16]$$

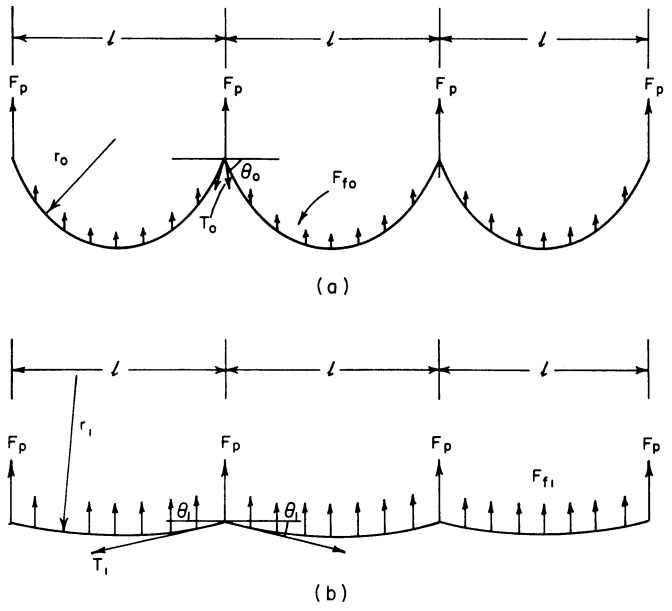

FIGURE 18. Comparison between (a) slow-moving and (b) fast-moving dislocation.

where B is the viscous damping coefficient and v the velocity of the dislocation. Peach-Koehler's equation states that, if the applied stress is ideally oriented:

$$F_{Ap} = \tau_{Ap} b \qquad [17]$$

F_p is independent of velocity, at high enough velocities (no diffusion needs to be considered) and can be computed from the energy of the vacancies (or interstitials) generated. If E_p is the energy of the point defect, and one defect is generated if the jog advances by b, one has

$$W = E_p = F_p b \qquad [18]$$

Hence:

$$F_p = \frac{E_p}{b} \qquad [19]$$

F(r) is the back force due to the circular shape of the dislocation. It can be expressed as:

$$F(r) = \frac{E_d}{r} \qquad [20]$$

where E_d is the energy of the dislocation line. The energy of the dislocation line is,in its turn, dependent on its velocity. Weertman has treated this subject in detail (47).

$$E_d = E_{d_o} \left[1 - \frac{v^2}{c^2} \right]^{-1/2} \qquad [21]$$

E_d and E_{do} are the self-energies of the dislocation at rest and at velocity v, respectively, and c is the velocity of elastic shear waves in the metal. Substituting Equations 16 through 21 into Equation 15:

$$\tau_{AP} b - Bv - \frac{E_p}{b\ell} - \frac{E_{d_o}}{r} \left[1 - \frac{v^2}{c^2} \right]^{-1/2} = 0$$

$$r = \frac{E_{d_o} \left[1 - \frac{v^2}{c^2} \right]^{-1/2}}{\tau_{Ap} b - Bv - \frac{E_p}{b\ell}} \qquad [22]$$

And:

$$\lim_{v \to c}(r) = \infty$$

This leads to the following significant conclusion: as the velocity increases, the effectiveness of jogs as barriers to dislocation motion decreases. They are effectively "dragged along" by the dislocation, generating in the process a large number of point defects. The same conclusion can be arrived at qualitatively by comparing Figure 18(a) and (b). It is even possible to estimate the concentration of point defects generated if one knows the density of dislocations generated and the amount that each dislocation will move. A simplified model is developed below. The number of jogs per unit length of dislocations is estimated from the number of intersections with other dislocations. If the distance between adjacent layers is d (equal to the distance between dislocation duplets at the front), and if each dislocation moves by a distance ℓ, it will have ℓ/d^2 jogs per unit length, at the end of its trajectory. The average distance by which a jog was dragged along is $\ell/2$. If one point defect is generated for each displacement equal to b, the total number N of point defects generated per dislocation is:

$$N = K \frac{\ell}{d^2} \left(\frac{\ell}{2}\right) \left(\frac{1}{b}\right) = \frac{K \ell^2}{2\, b d^2} \qquad [23]$$

The factor K was introduced to account for the fact that only a certain percentage of the intersections generate jogs that cannot move conservatively. To a first approximation, one can take K as 0.25. The total dislocation density being ρ, the concentration of point defects generated by shock loading is:

$$C = \frac{K \rho \ell^2}{2b\, d^2 n} \qquad [24]$$

n is the number of atoms per unit volume. But $1/d^2$ is equal to the dislocation density and

$$C = \frac{K \rho^2 \ell^2}{2nb} \qquad [25]$$

Some of these parameters are not known, at present, and some very rough approximations will be made. Making the calculation for nickel shock loaded at 20 GPa, one finds (35) that ρ is approximately 5×10^{10} cm^{-2}; b is 3.5 A; K is 0.25; n is approximately 2.5×10^{23} cm^{-3}; from (35) it was calculated that ℓ is equal to 0.7 μm. The input of these parameters provides

$$C = 7 \times 10^{-5}$$

Kressel and Brown (39) estimate the sum of vacancy and interstitial concentration to be approximately equal to this value. The closeness between calculated and measured point defect densities seems to indicate that the critical assumptions in the calculation, the distance ℓ = 0.7 μm is reasonable.

V. DEFORMATION TWINNING

A. Effect of Material and Shock-Wave Parameters

The most important and self-consistent comment that can be made about deformation twins is that twinning is a highly favored deformation mechanism under shock loading. Metals that do not twin by conventional deformation at ambient temperature can be made to twin by shock loading. In this respect, as in the morphology of dislocation substructures, shock deformation resembles conventional deformation at low temperature: loose cell walls and a greater tendency towards twinning. The ease of twinning depends on several factors:

(a) *pressure* - Nolder and Thomas (48,49) found that twinning occurred, in nickel, above 35 GPa pressure. This was generally confirmed by Greulich and Murr (50). DeAngelis and Cohen (51) found the same effect (a treshold pressure) in copper.

(b) *crystallographic orientation* - it is the deviatoric component of stress that induces twinning. Hence, when the resolved shear stress in the twinning plane and along the twinning direction reaches a critical level, twinning should occur. DeAngelis and Cohen (51) found an orientation dependence for the threshold stress; copper single crystals twinned at 14 GPa when the shock wave travelled along [100] and at 20 GPa when it travelled along [111]. Greulich and Murr (50) found for nickel that, at and above 35 GPa twinning occurred preferentially for [100] grains. As the pressure was increased the preponderance of twins increased along orientations other than [100].

(c) *stacking-fault energy* - as the S.F.E. of FCC metals is decreased, the incidence of twinning increases. As a corollary the treshold stress for twinning should decrease.

(d) *pulse duration* - the effect of pulse duration, first explored by Appleton and Waddington (16), was systematically investigated by Champion and Rohde (53) for an austentic (Hadfield) steel. They found striking differences in twin densities for different pulse durations, at 10 GPa. Numerous twins were observed at 2 μs, while no twinning was present at 0.065 μs. They concluded that there must be a treshold time for twinning. Staudhammer and Murr (54,55) investigated the effect of pulse duration (0.5, 1, 2, 6, 14 μs) on the substructure of AISI 304 stainless steel.

They found an increase in twin density up to about 2 μs; beyond that the twin density seemed to be essentially constant. Stone et al. (56) found,systematically, an increase in twin density as the pulse duration was increased from 0.5 to 1.0 μs, in both the AISI 1008 steel and Armco magnetic ingot iron. The twins generated by the shock pulse should not be confused with the ones formed by the elastic precursor wave, in iron; the latter ones were investigated by Rohde and coworkers (57,58). Although twins are generated by the elastic precursor waves, the volume percent of twins generated by the shock wave is an order of magnitude higher. While the elastic precursor may produce a twin density of 3 vol. pct.,a shock wave of 30 GPa peak pressure and 1 μs pulse duration has been shown to generate about 50 vol. pct. of twins.

(e) *existing substructure* - Rohde, et al.(59) found profuse twinning upon shock loading titanium - gettered iron in the annealed condition. However, predeformed samples exhibiting a reasonable density of dislocations did not twin. The same results were obtained by Mahajan (60) for iron. Hence, if one looks at dislocation generation and motion, and twinning as competing mechanisms, one can rationalize this response. The deviatoric stresses generated by a shock wave are accommodated by twinning when no dislocations are available and by motion of the already existing dislocations, if iron is predeformed.

(f) *grain size* - Murr et al.(61) were able to explain conflicting data reported in the literature (62,63) on the incidence of twinning in molybdenum by showing that, at a certain pressure, large-grain sized specimens twinned more readily than small-grain sized ones. However, it should be emphasized that this response is not unique to shock loading; indeed, iron - 3 pct silicon (65) and chromium (66) have been shown to exhibit a strong grain-size dependence of the twinning stress (in conventional deformation). Kestenbach and Meyers (52) investigated the effect of grain size on the substructure of AISI 304 stainless steel.

B. Mechanisms

The crystallographic and morphological features of shock-induced twins do not differ substantially from the conventionally-formed ones. Figure 19 shows representative twins in molybdenum (BCC) and nickel (FCC). In molybdenum they have a characteristic lenticular shape, while in nickel they resemble elongated arrays of stacking faults. Indeed,Murr and Grace (64) and Murr and Staudhammer (53) have demonstrated that deformation twins in shock-loaded FCC materials of low stacking-fault free energy are formed by overlapping intrinsic stacking faults on every {111} plane. Irregularities always occur forming twin-faults.

The rationale of considering twinning and slip by dislocations as competive processes is a fair and helpful one. It is well

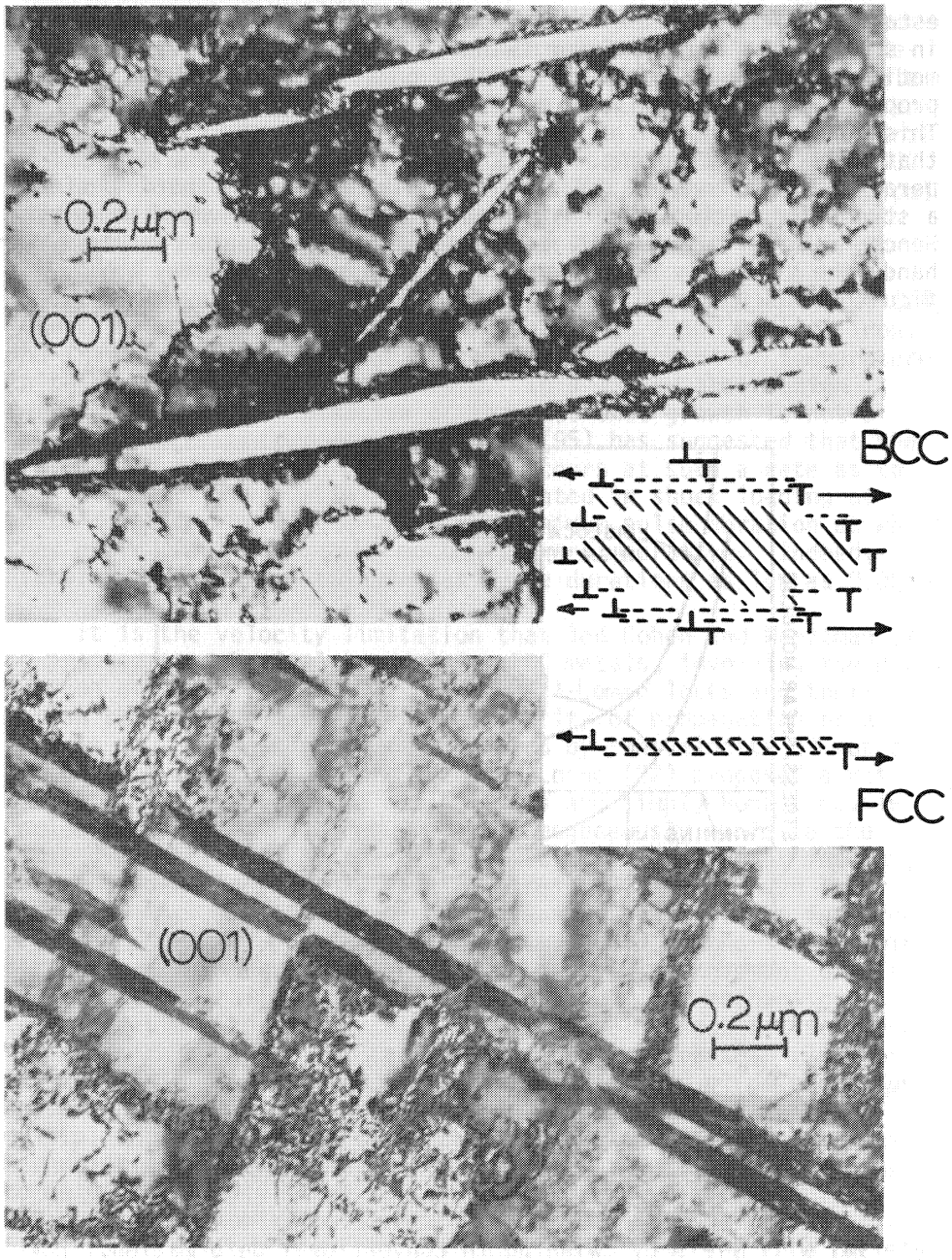

FIGURE 19. Comparison of shock-induced twin morphologies in BCC (molybdenum) and FCC (nickel) metals with corresponding simple twinning models involving systematic movement of dislocations on appropriate slip planes.

established that either a decrease in temperature or an increase in strain rate tend to favor twinning over slip by dislocation motion (e.g., Peckner (67)). In this context, the graphical scheme proposed by Thomas (68) for martensite can be generalized (69). This generalization is extended here to high strain rates, showing that they favor twinning. It is shown in Fig. 20. The low-temperature dependence of the stress required for twin initiation is a strong indication that it is not a thermally-activated mechanism. Hence, τ/G for twinning is not temperature dependent. On the other hand, the thermally activated dislocation motion becomes very difficult at low temperatures; T_t is the temperature below which the

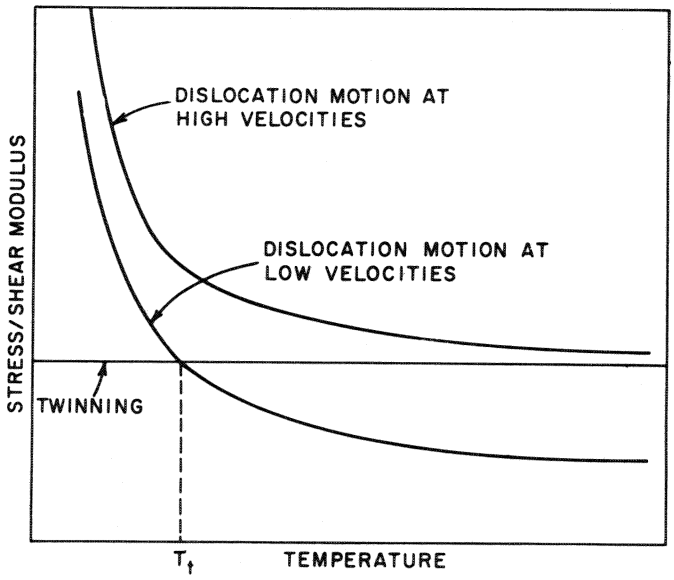

FIGURE 20. Effect of temperature on the stress required for twinning and slip (at low and high strain rates).

material will yield by twinning in conventional deformation. However, at high strain rates and in shock loading, dislocation generation and dynamics are such that the whole curve is translated upwards, while the twinning curve is stationary, for reasons that will be given later. As a consequence, the interaction of the two curves takes place at a higher temperature.

The fact that deformation twins exhibit similar crystallografic and morphological features in both conventional and shock deformation leads to the conclusion that the mechanisms responsible for the nucleation and growth should be similar. There are essentially two schools-of-thought regarding twin formation. The first is the pole mechanism proposed by Cottrell and Bilby (70) for BCC metals and extended by Venables (71) to FCC metals. The principal deterrent to the pole mechanism, especially in shock loading, is the maximum rate of growth predicted by this model; it is of the order of 1 ms^{-1}. This is about three orders of magnitude below values reported by Bunshah (72), Reid et al.(73), and Takeuchi (74). Takeuchi (74) found that a twin propagated at 2,500 ms^{-1} in iron, and that this velocity was virtually independent of temperature in the interval - 196°C to + 126°C. This latter observation is very important and indicative of the fact that growth is not a thermally activated process. Hornbogen (95) has suggested that the propagation of twins in Fe-Si alloys occurs at such a rate as to generate shock waves. Twins are generated in shock loading at pulse durations much lower than the minimum pulse duration at which they could grow, if a pole mechanism were operative. Indeed, Mikkola (76) observed twinning at pulse durations as low as 0.06 μs.

It is the velocity limitation that led Cohen and Weertman (76) to propose a much simpler model for FCC metals, involving the production of Shockley partials at Cottrell-Lomer locks and their motion through the material. The velocity of propagation of a twin is in this case simply established by the velocity of motion of the Shockley partials. Hirth and Lothe (22) proposed a yet simpler model in which the dislocations are simply homogeneously nucleated; while stress required to homogeneously nucleate the first dislocation is of the order of 10 pct of the shear modulus, the subsequent loops would require stresses that are much lower (1 pct of G). This "homogeneous nucleation" concept was forwarded first by Orowan (78). It is the feeling of the authors that twinning occurs in shock loading by the cooperative movement of dislocations on parallel planes. By comparison, the mechanism of twin formation proposed by Sleeswyk (79) for BCC materials is phenomenologically identical to that of Cohen and Weertman (76) for FCC materials, except that it involves systematic glide of dislocations on {112} planes and takes into account the slip plane multiplicity in BCC. It is especially convincing that these basic mechanistic models characterizing twinning in BCC and FCC appear to be geometrically identical to the actual twin morphologies observed by transmission electron microscopy. These features are illustrated by comparing the schematic model inserted into the twin images shown in Fig. 19.

It is likely that twins in low stacking-fault free energy metals and alloys can form at ledges in the grain boundaries as previously described by Meyers and Murr (80), or at ledges formed

on other interfaces (such as annealing twins, other deformation twins, epsilon phase, etc.) or at intersections of dislocations which form the Burgers vector characteristic of a ledge (81). Figure 21 illustrates the association of shock-induced stacking faults, twins, and twin-faults in 304 stainless steel with annealing twin boundaries and grain boundaries.

The twins formed by the cooperative movements of dislocations as shown in Fig. 19 are normally irregular in shock-induced materials. That is, the glide of individual dislocations can be interrupted (impeded), and this can produce a change in the stacking array as described earlier by Murr and Grace (64). This means that a twin which propagates within a grain may contain stacking irregularities giving rise to thin ε-phase or individual stacking faults. Indeed, the formation of intrinsic stacking faults on every {111} plane produces the twin while formation on every other {111} plane will give rise to the HCP (ε) phase. Consequently,

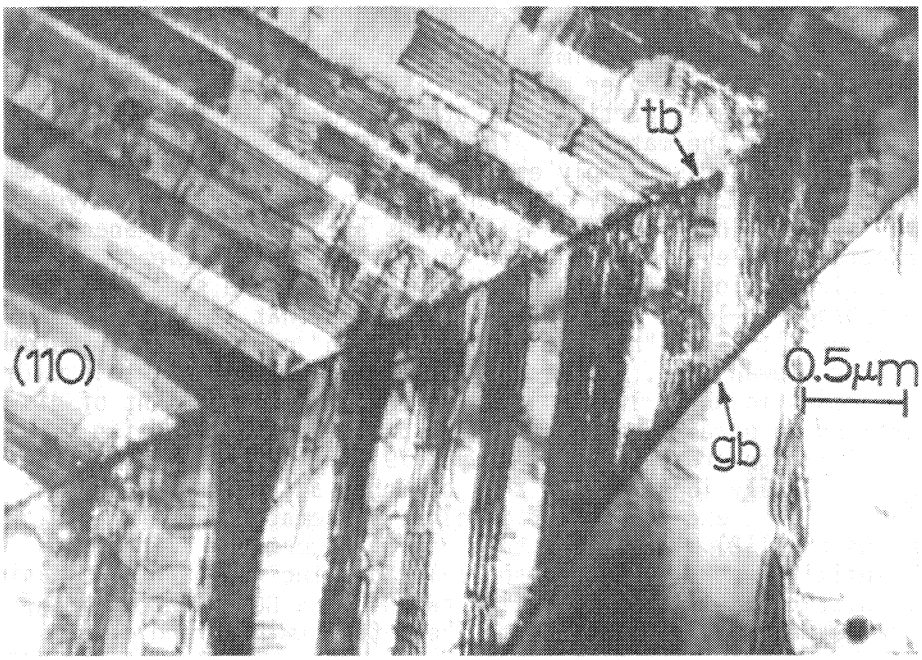

FIGURE 21. Shock-induced stacking faults and twin faults in 304 stainless steel shock-loaded at 15 GPa peak pressure, 2 μs pulse duration. Note annealing twin and grain boundaries associated with the faults.

the twin volume when viewed selectivity by dark-field electron microscopy, often appears irregular. This feature is illustrated in Fig. 22 which shows well-formed twins in shock-loaded nickel which are irregular in contrast when viewed with a selective twin reflection as shown in the corresponding selected-area electron diffraction pattern.

Since dislocation emission and the activation of glide processes are pressure dependent, it would be expected that at lower pressures only a few stacking faults or thin twins would be formed, with increasing numbers and sizes (thicknesses) of twins occurring with increasing shock pressure. In effect, the volume fraction of twinned material is expected to increase with shock pressure. In addition, in low stacking-fault free energy materials in particular, low shock pressures would create single and small arrays of overlapping faults (as shown in Fig. 21) which would be expected to increase with increasing shock pressure, creating more well-defined twins (or twin-faults). These features are illustrated in the sequence of electron micrographs for shock-loaded type 304 stainless steel shown in Fig. 23.

VI. DISPLACIVE/DIFFUSIONLESS TRANSFORMATIONS

There are numerous instances in which a shock wave induces a phase transformation. A very detailed review is presented by Graham and Duvall (82); for this reason, only a classification scheme will be presented here. The phase transformations involving diffusion are excluded from this discussion. Stein (83) has shown that precipitation is induced by shock loading; however, it was not possible to establish whether this transformation took place during or after the passage of the shock wave; the latter hypothesis is more probable.

Cohen et al.(84) proposed recently a classification scheme for displacive/diffusionless transformations. The first division is between shuffle and lattice-distortive transformations; the latter group is divided into two sub-groups; dilatation - dominant and deviatoric - dominant transformations. The term martensitic (and quasi-martensitic) is reserved for the lattice-distortive transformations in which the deviatoric component of stress is dominant. Hence, only the FCC → BCC (or BCT) and FCC → HCP transformation in the Fe-base alloys and the BCC → close packed transformations in the noble metal alloys can, *strictu sensu*, be called martensitic. A whole range of phase transformations, such as the beta-omega in Ti alloys and the tetragonal - cubic transformation in tin, cannot be called martensitic.

The effect of a shock pulse on a displacive/diffusionless transformation has to be analyzed from three points - of - view:

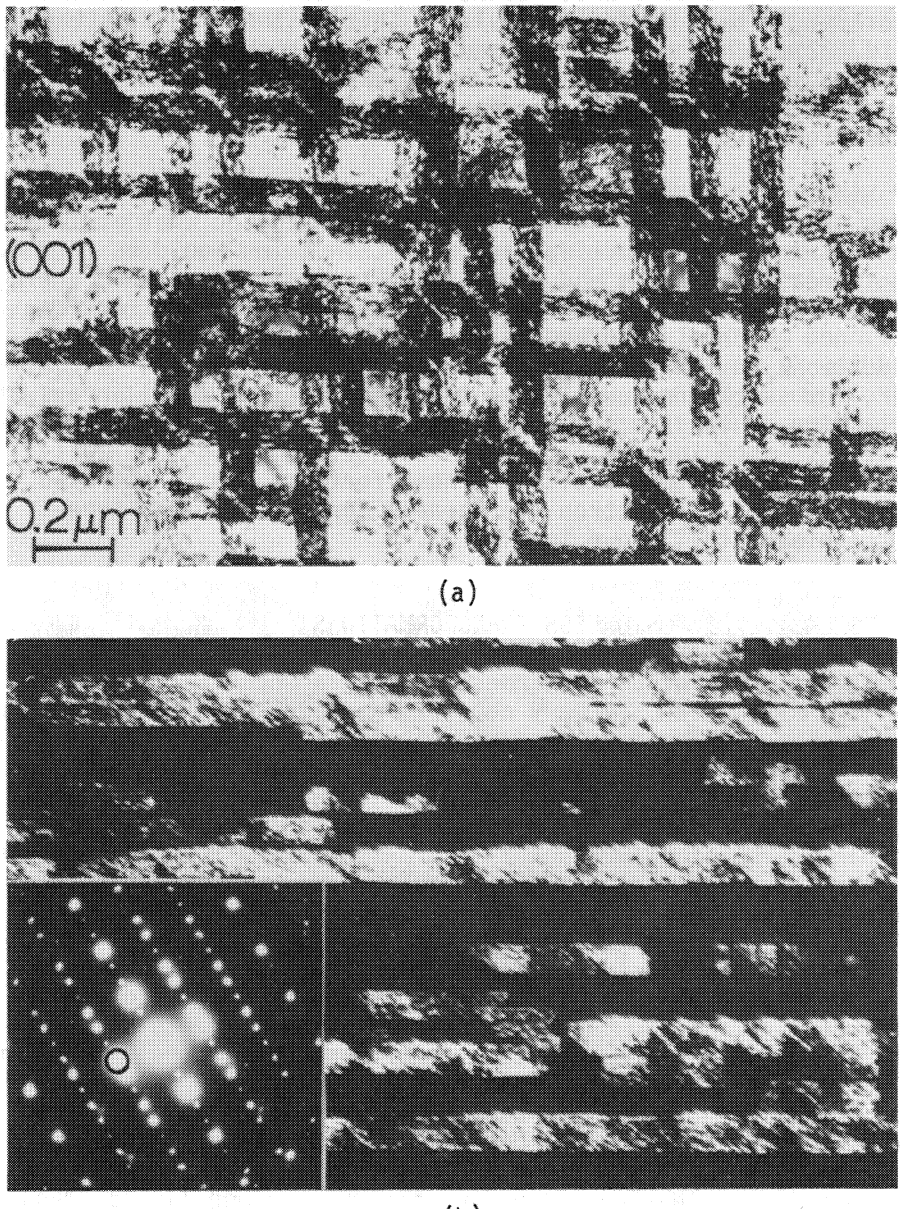

FIGURE 22. Deformation twins in shock-loaded nickel (45 GPa peak pressure, 2 μs pulse duration). (a) Bright-field electron transmission image. (b) Dark-field image using the twin spot shown in the selected-area electron diffraction pattern insert. Note the contrast irregularities along individual twins.

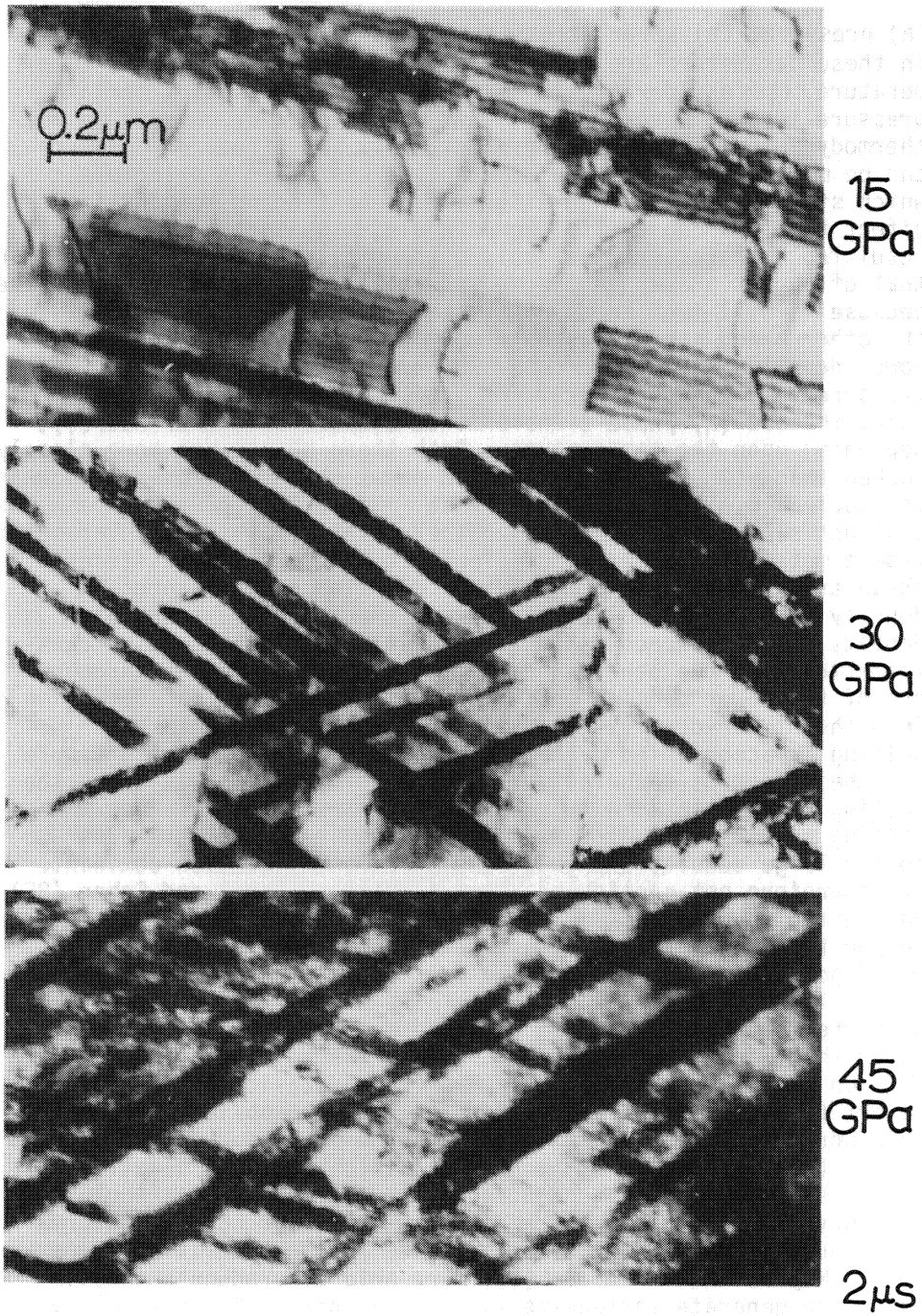

FIGURE 23. Dependence of twin volume fraction on peak pressure in shock-loaded AISI 304 stainless steel.

(a) pressure; (b) shear stresses and (c) temperature. The changes in these parameters are not independent; there are specific temperature rises and deviatoric stresses associated with a certain pressure level. Nevertheless, they have different effects on the thermodynamics of phase transformations. The effect of pressure can be more clearly seen in light of Le Chatelier's principle which states that a change will take place tending to minimize the effect that has caused it. For example, a phase transformation resulting in a reduction of volume (density of product greater than that of parent phase) is thermodynamically favored at high pressure, because it will tend to decrease the pressure on that region. On the other hand, a phase transformation in which the product has a lower density is not favored by the pressure. Figure 24 shows the pressure-temperature diagram for iron. At a certain critical pressure, the BCC (α) phase transforms to either HCP (ε) or FCC (γ), depending upon the temperature. Both these phases are more closely packed than α(BCC). Figure 24 also shows that the pressure increase is coupled to a temperature increase. Hence, the pressure path has a slight slope. Plutonium is another metal that is very interesting from a metallurgical point of view. It undergoes six different phase transformations, some of them with large differences in density (86). The room-temperature monoclinic phase has a high density (19.86); hence, the pressure will not induce phase transformation. On the other hand, if the shock wave passes through one of the lower density phases, it will favor its transformation into the higher-density phases. Plutonium is unique in that melting is accompanied by a volume decrease. Hence, the pressure has the effect of reducing the melting point; in metals where the melting is associated with an expansion, pressure increases the melting point. Some of the transformations in Pu alloys are, due to the large density changes, considered as dilatation-dominant, are therefore not considered as martensitic. Patel and Cohen (85) have established a rationale for the effect of stresses on the M_S temperature in martensite transformations. They found that, in Fe-30 pct alloy, the hydrostatic pressure decreased the M_S temperature. In these alloys, there is a dilatation of 5 pct associated with the martensitic phase. Hence, a pressure pulse should not favor the transformation, and this is reflected in the decrease in M_S. On the other hand, an alloy in the martensite form should revert to austenite, if a pressure pulse were applied, because this would result in a contraction of the lattice. Indeed, Rohde (87) was able to confirm this effect. A negative pressure pulse, inducing negative hydrostatic pressures would be the converse situation and the γ(FCC) $\rightarrow$ α(BCC or BCT) transformation would be favored, with an increase in the transition temperature. Meyers and Guimaraes (88) were able to produce a tensile pulse and generate martensite in an Fe-31 pct Ni-0.1 pct alloy

Figure 25 shows the martensite tube generated by tensile waves, this tensile wave was produced by a compressive shock wave, as it

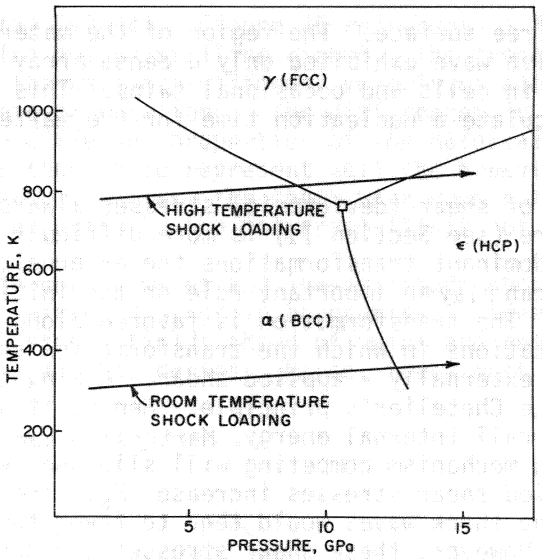

FIGURE 24. Temperature-pressure diagram for iron.

FIGURE 25. Martensite generated by tensile hydrostatic stresses produced by a reflected pressure pulse in iron-nickel alloy(88).

reflected at a free surface. The region of the material traversed by the compressive wave exhibited only a dense array of dislocations organized in cells and occasional twins. This phenomenon was used to calculate a nucleation time for the martensitic transformation (89).

The effect of shear (deviatoric) stresses always associated with the pressure (see Section II) is more difficult to assess. In deviatoric - dominant transformations the externally applied shear stresses can play an important role on the initiation of transformation. The transformation is favored along the crystallographic orientations in which the transformation shear will tend to decrease the externally - applied shear. Again, this is the application of Le Chetelier's principle. Hence, it will tend to decrease the overall internal energy. Martensite can be considered as a deformation mechanism competing will slip and twinning, and externally applied shear stresses increase M_S. The shear stresses introduced at the shock waves would tend to favor the generation of martensite. However, these shear stresses are much lower than the hydrostatic stresses for most shock waves, because dislocation nucleation and twinning will attenuate them. Hence, these shear stresses will only generate martensite when the temperature at the shock front is only slightly higher than M_S. In this case, martensite transformation can effectively compete with twinning and slip. Olson and Cohen (90) have shown that, during conventional deformation at temperatures slightly below M_S, yielding is produced by stress-induced martensite. The same phenomenon was confirmed by Guimaraes et al (91): Up to 20 K above M_S, yielding was initiated by martensitic transmformation. Hence, one can conclude that the shear stressed associated with shock loading might be important in martensite nucleation if the temperature at the shock front is within 50 K of the M_S under the imposed conditions (at the level of pressure established by the shock pulse). These features are demonstrated by Staudhammer et al in Chapter 7 who also show that martensite forms exclusively in 304 stainless steel at the intersections of twin-faults.

VII OTHER EFFECTS

There a number of additional effects due to the fact that the shock wave does not traverse an idealized monocrystalline metal but a medium in which there may be grain boundaries, twin boundaries, precipitates, and other microstructural features. They all affect the propagation of the shock wave and the generation of defects, to a smaller or larger extent. The realization that the anisotropy of elastic and plastic properties of the individual grains in a polycrystal led to a "wavy wave" model, which attempted to represent the irregularities in both the front and peak pressure of the elastic precursor and shock wave as they propagate through-

out of the metal (92-94). Figure 26 represents a "wavy-wave" front after traversing polycrystalline nickel. The front becomes irregular because the wave has different velocities along different crystallographic orientations. The differences in peak pressure are due to the different properties of the material. The "wavy-wave" model is thought to represent well the behavior of the elastic precursor; however, the shock wave does not seem to be significantly affected by the polycrystallinity of the material.

Elastic precursor waves and low-amplitude shock waves are also reflected and refracted at grain boundaries. Indeed, Hornbogen (95) has shown that stress fields ahead of twins are reflected and diffracted at grain boundaries. Hence, there must be regions

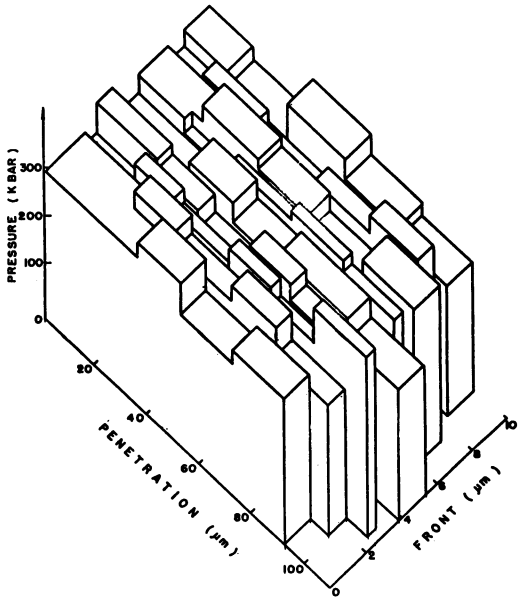

FIGURE 26. Proposed model for shock wave (shock front at about 100 μm below surface).

where the pressures are below the average value. During the passage of the pulse there must be also pulse irregularities propagating along different directions. These effects are, however, of secondary importance for very high amplitude pressure pulses.

Second-phase particles can play a significant role in the generation of defects. This can be explained from two angles. First, if the particle has a different elastic modulus than the matrix, the hydrostatic componenet of the stress will produce interface stresses that will lead to the "punching out" of dislocations. Indeed, Das and Radcliffe (96) have observed this effect when applying hydrostatic pressure by conventional means to metals containing particles. The same process is certainly operative during shock loading. Second, the shock front is reflected, refracted, disturbed when passing through the particle. This is eloquently illustrated in Figure 27 from Leslie et al. (97). The inclusion has a clear effect on the distribution of deformation twins. The region "down stream" of the inclusion exhibits a higher DPH hardness (417) than the average value (~ 280). It is clear that the inclusion - matrix interface or the dislocations at the adjoining region acted as nucleation sites for additional twinning, responsible for the greater hardness.

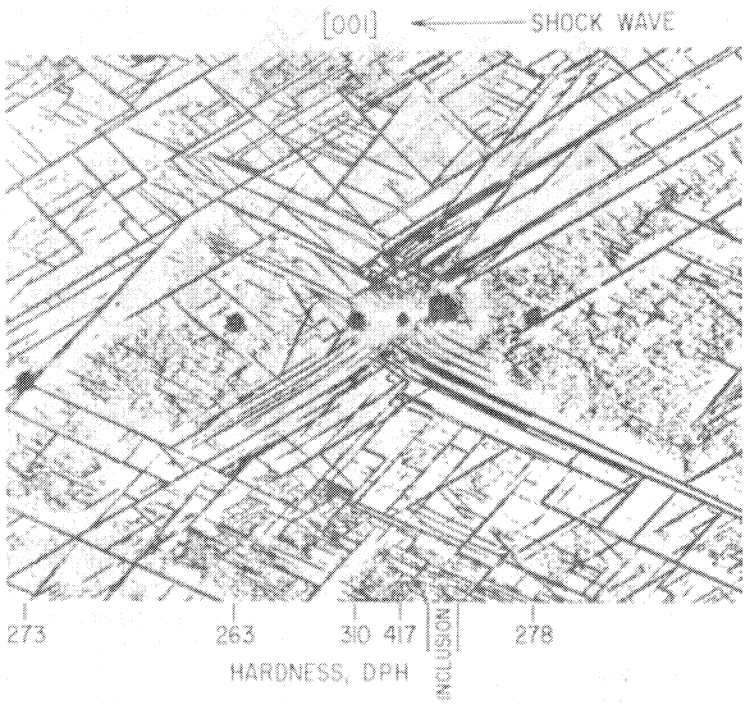

FIGURE 27. Hardness readings near an inclusion in a shock-loaded Fe-3% Si single crystal. Nital etch x 140 (97).

There are additional effects of pressure that have not been considered in this review but that are worthy of analysis, since they have certainly a bearing on the residual substructure of shock-loaded metals. Noteworthy among these are the effects of pressure and shear stress on the stacking-fault energy, on the diffusion coefficient, and on the mobility of dislocations.

VIII ACKNOWLEDGMENTS

The writing of this manuscript was supported by NSF Grant No DMR 7977102. Some of the activities which compose this chapter were also supported by the Research and Development Division of New Mexico Tech.

IX REFERENCES

1. Rinehart, J.S. and Pearson, J., "Behavior of Metals Under Impulsive Loads", ASM, Cleveland, Ohio, 1954.
2. Smith, C.S., *Trans. AIME*, 212, 574 (1958).
3. Dieter, G.E., in "Strengthening Mechanisms in Solids", ASM, Metals, Park, Ohio, p. 279, 1962.
4. Dieter, G.E., in "Reponse of Metals to High-Velocity Deformation", eds., P.W. Shewmon and V.F. Zackay, p. 409, Interscience, New York, 1961.
5. Zukas, E.G., *Metals Eng. Quart.*, May, 6, 1 (1966).
6. Otto, H.E. and Mikesell, R., First Intl. Conf. Center for High Energy Rate Forming, U. of Denver, Colorado, June, 1967.
7. Orava, R.N., in "Principles and Practice of Explosive Metalworking", Fuel and Metallurgical Journal, London, p. 229 ,1973.
8. Leslie, W.C., in "Metallurgical Effects at High Strain Rates", eds., R.W. Rohde, B.M. Butcher, J.R. Holland, and C.H. Karnes, p. 571, Plenum, New York, 1973.
9. Davison, L. and Graham, R.A., *Physics Reports*, 55, 255 (1979).
10. De Carli, P.S. and Meyers, M.A., Chap. 22, this volume.
11. Wasley, R.J., "Stress Wave Propagation in Solids", Marcel Dekker, New York, 1973.
12. Dieter, G.E., "Mechanical Metallurgy", 2nd ed., p. 53, McGraw-Hill, New York, 1976.
13. Appendix F, pp. 1059, this volume.
14. Bridgman, P.W., "The Physics of High Pressure", MacMillan, p. 386, New York, 1931.
15. Jesser, W.A. and Kuhlmann-Wilsdorf, D., *Mat. Sci. and Eng.*, 9, 111 (1972).
16. Appleton, A.S. and Waddington, J.S., *Acta Met.*, 12 681 (1963).
17. Duvall, G.E. and Graham, R.A., *Rev. of Modern Physics*, 49, 523 (1977).
18. Murr, L.E. and Wilsdorf, D. Kuhlmann, *Acta Met.*, (1978).
19. Meyers, M.A., *Met. Trans.*, 8A, 1641 (1977).

20. Marsh, E.T. and Mikkola, D.E., *Scripta Met.*, 10, 851 (1976).
21. Dhere, A.G., M. Sc. thesis, Instituto Militar de Engenharia, Rio de Janeiro, Brasil, 1978.
22. Leslie, W.C., Michalak, J.T., and Aul, F.W., in "Iron and Its Dilute Solid Solutions", p. 119, J. Wiley, New York, 1963.
23. Koul, M.K. and Breedis, J.F., in "The Science, Technology, and Application of Titanium", eds. R.I. Jaffee and N.E. Promisel, p. 817, Pergamon Press, Oxford, 1978.
24. Galbraith, J. and Murr, L.E., *J. Matls. Sci.*, 10, 2025, (1975).
25. Hornbogen, E., *Acta Met.*, 10, 978 (1962).
26. Talia, E., Fernandez, L. Sethi, V.K., and Gibala, R., in source cited in ref. 28, p. 127.
27. Sestak, B., source cited in ref. 28, p. 1461.
28. Meyers, M.A., in "Strength of Metals and Alloys", eds. P. Haasen, V. Gerold, and G. Kostorz, p. 547, Pergamon Press, New York, 1979.
29. Rohde, R.W. and Pitt, C.H., *J. Appl. Phys.*, 38, 876 (1967).
30. Friedel, J., "Dislocations", p. 63, Addison-Wesley, New York, 1964.
31. Meyers, M.A., *Scripta Met.*, 12, 21 (1978).
32. Taylor, J.W., *Appl. Phys.*, 34, 2727 (1963).
33. McQueen, R.J., Zukas, E.G., and Marsh, S.P., "Residual Temperature in Shock Loaded Iron", ASTM STP No. 336, p. 306, 1962.
34. Hirth, J.P. and Lothe, J., "Theory of Dislocations, McGraw Hill, New York, p. 689, 1968.
35. Hsu, K.C., Hsu, C.Y., Murr, L.E., and Meyers, M.A., Chap. 27, this volume.
36. Kazmi, B., and Murr, L.E., Chap. 41, this volume.
37. Mogilevskii, M.A., Proceedings of the Symposium on High Dynamic Pressure, Paris, August (1978).
38. Mogilevskii, M.A., Chap. 31, this volume.
39. Kressel, H. and Brown, N., *J. Appl. Phys.*, 38, 138 (1967).
40. Brillhart, D.C., DeAngelis, R.J., Preban, A.G., Cohen, J.B., and Gordon, P., *Trans. AIME*, 239, 836 (1967).
41. Rose, M.F. and Berger, T.L., *Phil. Mag.*, 17, 1121 (1968).
42. Styris, D.L. and Duvall, G.E., *High Temp. - High Press.*, 2, 477 (1970).
43. Ginsberg, M.J. and Grady, D.E., *Bull. Am. Phys. Soc.*, 17, 477 (1970).
44. Christou, A., *Phil. Mag.*, 26, 97 (1972).
45. Dick, J.J. and Styris, D.L., *J. Appl. Phys.*, 46, 1602 (1975).
46. Murr, L.E., Inal, O.T., and Morales, A.A., *Acta Met.*, 24, 261, (1976).
47. Weertman, J., in "Response of Metals to High Velocity Deformation", eds., P.G. Shewmon and V.F. Zackay, p. 205, Interscience, New York, 1961.
48. Nolder, R.L. and Thomas, G., *Acta Met.*, 11, 994 (1963).
49. Nolder, R.L. and Thomas, G., *Acta Met.*, 12, 227 (1964).
50. Greulich, F. and Murr, L.E., *Mat. Sci. and Eng.*, 39, 81 (1979).

51. DeAngelis, R.J. and Cohen, J.B., *J. Metals*, 15, 681 (1963).
52. Kestenbach, H.-J. and Meyers, M.A., *Met. Trans.*, 7A, 1943 (1976).
53. Champion, A.R. and Rohde, R.W., *J. Appl. Phys.*, 41, 2213 (1970).
54. Staudhammer, K.P. and Murr, L.E., Proc. 5th Intl. Conf. on High Energy Rate Fabr., U. of Denver, Colorado, p. 1.7.1, 1975.
55. Murr, L.E. and Staudhammer, K.P., *Mat. Sci. and Eng.*, 20, 95, (1975).
56. Stone, G.A., Orava, R.N., Gray, G.T., and Pelton, A.R., "An Investigation of the Influence of Shock-Wave Profile on the Mechanical and Thermal Responses of Polycrystalline Iron", Final Technical Report, U.S. Army Research Office, Grant No. DAA629-76-0181, p. 30, 1978.
57. Rohde, R.W., *Acta Met.*, 17, 353 (1969).
58. Johnson, J.N. and Rohde, R.W., *J. Appl. Phys.*, 42, 4171 (1971).
59. Rohde, R.W., Leslie, W.C., and Glenn, R.C., *Metall. Trans.*, 3A, 323 (1972).
60. Mahajan, S. *Phys. Stat. Sol.*, 33, 291 (1969).
61. Wongwiwat, K. and Murr, L.E., *Mater. Sci. Engr.*, 35, 273 (1978).
62. Verbraak, C.A., "Science and Technology of W, Ta, Mo, Nb, and Their Alloys", Pergamon Press, N.Y., 1964, p. 219.
63. Murr, L.E., Inal, O.T., and Morales, A.A., *Appl. Phys. Letters*, 28, 432 (1976).
64. Murr, L.E., and Grace, F.I., *Exptl. Mechs.*, 9, 145 (1969).
65. Marcinkowski, M.J. and Lipsift, H.A., *Acta Met.*, 10, 951 (1962).
66. Hall, D., *Acta Met.*, 9, 191 (1961).
67. Peckner, D., "The Strengthening of Metals", Reinhold, New York, p. 49, 1964.
68. Thomas, G., *Met. Trans.*, 2, 2373 (1971).
69. Thomas, G., Univ. of California, Berkeley, private communications (1978).
70. Cottrell, A.H. and Bilby, *Phil. Mag.*, 42, 573 (1951).
71. Venables, J.A., *Phil. Mag.*, 6, 379 (1961).
72. Bunshah, R.F., in "Deformation Twinning", eds. Reed Hill, R.E., Hirth, J.P., and Rogers, H.C., Gordon and Breach, New York, p. 390, 1964.
73. Reid, C.N., Hahn, G.T., and Gilbert, A., Source cited in ref. 72, p. 386.
74. Takeuchi, T., J. Phys. Soc. Japan, 21, 2616 (1966).
75. Wright, R.M., Mikkola, D.E., and LaRouche, S., Chap. 39, this volume.
76. Cohen, J.B. and Weertman, J., *Acta Met.*, 11, 997 (1963), 1368 (1963).
77. Hirth, J.P. and Lothe, J., "Theory of Dislocations", McGraw-Hill, New York, p. 750, 1968.

78. Orowan, E., "Dislocations in Metals", A.I.M.E., New York, p. 116, 1954.
79. Sleeswyk, A.W., *Acta Met.*, 10, 803 (1962).
80. Meyers, M.A., and Murr, L.E., *Acta Met.*, 26, 951 (1978).
81. Hirth, J.P. and Balluffi, R.W., *Acta Met.*, 21, 929 (1973).
82. Duvall, D.E. and Graham, R.A., *Reviews of Modern Phys.*, 49, 523 (1977).
83. Stein, C., *Scripta Met.*, 9, 67 (1975).
84. Cohen, G.B. and Cohen, M., *J. Less Common Metals*, 28, 107 (1972).
85. Patel, J.R. and Cohen, M., *Acta Met.*, 1, 531 (1953).
86. Hecker, S.S., Los Alamos Scientific Laboratory, private communication (1979).
87. Rohde, R.W., Holland, J.R., and Graham, R.A., *Trans. Met. Soc. AIME*, 242, 2017 (1968).
88. Meyers, M.A. and Guimaraes, J.R.C., *Matls. Sci. and Eng.*, 24, 289 (1976).
89. Meyers, M.A., *Met. Trans.*, 10A, 1723 (1979).
90. Olson, G.B. and Cohen, M., *J. Less Common Metals*, 28, 107 (1972).
91. Guimaraes, J.R.C., Gomes, J.C., and Meyers, M.A., *suppl. to Trans., J.I.M.*, 1741 (1976).
92. Meyers, M.A., Proc. Fifth Intl. Conf. on High Energy Rate Fabrication, U. of Denver, Colorado, June 1975, p. 1.4.1.
93. Meyers, M.A. and Carvalho, M.S. *Matls. Sci. and Eng.*, 24, 131 (1976).
94. Meyers, M.A., *Matls. Sci. and Eng.*, 30, 99 (1977).
95. Hornbogen, E., *Trans. A.I.M.E.*, 221, 712 (1961).
96. Das, G. and Raddcliffe, S.V., *Phil. Mag.*, 20, 589 (1969).
97. Leslie, W.C., Stevens, D.W., and Cohen, M., in "High-Strength Materials", ed. V.F. Zackay, p. 382, John Wiley, New York, 1965.
98. Raikes, S. and Ahrens, T.J., *Geophys. J.R. Astr. Soc.*, 58, 717 (1979).

PRINTED IN U.S.A.